[redacted]

AEROSOL DEPOSITION FROM TURBULENT AIRSTREAMS IN VERTICAL CONDUITS

G. A. SEHMEL

MARCH, 1968

[redacted]

AEC RESEARCH & DEVELOPMENT REPORT

BATTELLE NORTHWEST
BATTELLE MEMORIAL INSTITUTE PACIFIC NORTHWEST LABORATORY
3000 STEVENS DRIVE, P. O. BOX 999, RICHLAND, WASHINGTON 99352

BNWL-578

LEGAL NOTICE

PACIFIC NORTHWEST LABORATORY
RICHLAND, WASHINGTON
operated by
BATTELLE MEMORIAL INSTITUTE
for the
UNITED STATES ATOMIC ENERGY COMMISSION UNDER CONTRACT AT(45-1)-1830

PRINTED IN/FOR THE U.S. ATOMIC ENERGY COMMISSION

54-1950-019 (11-67)
BEC-RL RICHLAND, WASH

BNWL-578
UC-41, Health and Safety

AEROSOL DEPOSITION FROM TURBULENT AIRSTREAMS IN VERTICAL CONDUITS

By

G. A. Sehmel

Atmospheric Sciences Section
Environmental and Radiological Sciences Department

March 1968

PACIFIC NORTHWEST LABORATORY
RICHLAND, WASHINGTON

Printed in the United States of America
Available from
Clearinghouse for Federal Scientific and Technical Information
National Bureau of Standards, U. S. Department of Commerce
Springfield, Virginia 22151
Price: Printed Copy $3.00; Microfiche $0.65

AEROSOL DEPOSITION FROM TURBULENT AIRSTREAMS IN VERTICAL CONDUITS

G. A. Sehmel

ABSTRACT

The general equations of continuity are set up to describe deposition of particles in which the eddy diffusivity is related to the Reynolds stress. Simplifying assumptions in the general equations as well as simplifying assumptions to obtain a workable model are discussed. The general equations are used as a basis from which to discuss existing models of turbulent deposition. A model is being developed for the case of deposition in tubes. Deposition velocities are shown using the initial assumptions for solving the model.

The deposition of 1 to 28 μ particles was measured in lengths of 0.21, 0.62, 1.152, and 2.81 in. ID aluminum tubes. Uranine or uranine-methylene blue particles of a narrow size range generated with a spinning disc aerosol generator were passed through the tubes. The deposition data are reported as deposition velocities for each tube size as a function of flow rate, or Reynolds number, and particle size.

Deposition velocities are from about 10^{-4} to 10 cm/sec. In general, for a given particle size and tube diameter, the deposition velocity remains low at about 10^{-4} cm/sec as the Reynolds number is increased above 2000 which is the flow transition region from laminar to turbulent flow. As flow becomes more turbulent, the radial motion of the particles becomes increasingly greater. This causes deposition to increase rapidly with Reynolds number. Above critical turbulent Reynolds number ranges, the deposition velocity increases rapidly as the Reynolds number is increased. These ranges of rapid initial increase start for Reynolds numbers from about 2,000 to 50,000. The Reynolds numbers required are a function of particles size and tube size. For further increases of Reynolds number, the deposition velocities increase to the order of 10 cm/sec.

At still higher Reynolds numbers, the apparent deposition velocity decreases below the order of 10 cm/sec due to particle re-entrainment from the tube surfaces. This decrease was observed to be down to an apparent deposition velocity as low as 10^{-3} cm/sec for the range of variables shown. For these same conditions, the deposition velocity will remain at about 10 cm/sec, if re-entrainment is minimized by covering the tube surface with a tacky coating. The tacky coating may also increase the deposition for the region in which the deposition velocity increases rapidly with Reynolds number. Conditions exist for which the deposition velocity for 2 μ diam particles is increased one magnitude by the tacky coating. This indicates that the 2 μ particles are re-entrainable.

TABLE OF CONTENTS

LIST OF FIGURES

AEROSOL DEPOSITION FROM TURBULENT AIRSTREAMS IN VERTICAL CONDUITS

G. A. Sehmel

INTRODUCTION

The purpose of the study reported herein was to determine the variables and their relationships which affect particle deposition to the walls of vertical conduits. These relationships will have direct immediate application to predicting deposition in lines transporting particles. Understanding of the basic mechanisms should lead to better understanding of deposition in the most general cases.

Deposition processes are the basic mechanisms by which particles are removed from an airstream. The effectiveness of these processes may be deliberately enhanced in air-cleaning systems. Natural deposition processes are effective in the environment in bringing airborne particles to rest.

These deposition processes are extremely important in assessing the significance of radioactive fallout, in determining the biological consequences of particles inhaled into the lungs, and in the design of effective air-cleaning devices. Deposition is similarly important in transporting particles in conduits or other passageways. It is important, therefore, that deposition processes be well understood to obtain the maximum benefit when deposition is beneficial or to minimize the deposition when it is harmful or undesirable.

SUMMARY

Particle deposition has been characterized by a deposition velocity, K, defined as the number of particles deposited per unit area per unit time per unit average concentration in the gas over the surface. Particles carried in an air stream through a conduit are deposited on the walls to a degree depending upon the deposition

velocity, tube length, tube diameter, the average velocity in the stream, the tube surface conditions, and perhaps other variables. The deposition velocity may be calculated from a simplifying particle mass balance around the tube from the model,

$$\ln \frac{C}{C_o} = -4\left(\frac{K}{V}\right)\left(\frac{L}{D}\right) \qquad (1S)$$

in which C is the average concentration of particles in the air at a distance, L, downstream of the initial entering concentration, C_o; V is the average air velocity; and D is the tube inside diameter.

Friedlander and Johnstone,[1] Owen,[2] and Davies[3-5] have proposed theories to predict the values of the deposition velocity from turbulent flow. These theories are discussed in terms of the general equation of continuity. In these theories, the assumption is made that particles will move toward the wall due to a particle turbulent diffusivity, ϵ_p. The particle diffusivity is used to calculate the flux of particles to the tube wall from the expression

$$N = -\epsilon_p \nabla C \quad . \qquad (2S)$$

In this expression, ∇C is the particle concentration gradient from some point in the flowing stream toward the wall. The assumption has always been made that the concentration of particles is maximum in the turbulent core, and that the concentration decreases as the tube wall is approached. The transport of particles to the tube wall has been explained in terms of the concentration gradient--particles go from a high concentration to a low concentration at a rate proportional to the particle diffusivity. Particles diffuse down the concentration gradient until they reach a distance from the wall equal to the stopping distance for the velocity the particles possess. Motion to the wall from this point is assumed to be by "free-flight". The free-flight or stopping distance is determined by particle size, gas velocity, viscosity, and other variables.

Air loadings of particles were measured as a function of radial distance from the center of a 2.81 in. ID tube when monodisperse particles were being carried in a turbulent flow. When the tube was coated to

provide a tacky surface, particle loading profiles were similar to velocity profiles as qualitatively anticipated. For many conditions, however, a higher flux of particles was moving down the tube very near the wall than out in the center of the tube. These "inverse" flux profiles are evidence that the diffusion of material from the central region of the tube to the wall cannot always be expressed by as simple a diffusion equation as that shown in Equation (2S). Theories developed to date thus fail to take into account all the parameters influencing net deposition, and this is especially true when rebounding and re-entrainment from the wall occurs. Marked rebounding or re-entrainment can be prevented by coating the internal surfaces of a tube with petroleum jelly which serves as a near perfect sink for particles. In these cases, the diffusional models should be more applicable. The deposition velocities for tacky surfaced tubes are much higher than for untreated tubes for many combinations of variables.

The deposition of 1 to 28-μ diam particles was measured in lengths of 0.21, 0.62, 1.152, and 2.81 in. ID aluminum tubes. Uranine or uranine-methylene blue particles of a narrow size range generated with a spinning disc aerosol generator were used. Deposition velocities are from about 10^{-4} to 10 cm/sec. In general, for a given particle size and tube diameter, for an as-received tube, the deposition velocity remains low at about 10^{-4} cm/sec as the Reynolds number is increased above the transition region at around 2000. Depending upon tube size and particle size, a rapid increase in deposition velocity as Reynolds number is increased occurs somewhere between Reynolds numbers from about 2,000 to 50,000.

The increase is to the order of 10 cm/sec and can occur over a small range of Reynolds numbers from 2000 to 5000, or over a large range of Reynolds numbers from 5,000 to 50,000. At still higher Reynolds numbers, the apparent deposition velocity decreases below the order of 10 cm/sec due to particle re-entrainment from the tube surfaces. This decrease was measured to apparent deposition velocities as low as 10^{-3} cm/sec for the range of experimental variables.

Experimental deposition velocities for 2-μ diam particles in a 0.21 in. ID tube are compared with those predicted from the models of

Friedlander and Johnstone, Davies, and the author. The comparisons indicate that the theories show some agreement, but theoretical predictions still need to be improved. Improved theory is being sought.

THEORETICAL DEVELOPMENT

We can derive equations to describe isothermal particle motion in air and the final surface deposition when end effects are unimportant. The equations will be developed for the general case and will then be simplified to the geometry of a vertical tube. The equations will be applicable to the cases in which the concentration decreases continuously as the wall is approached. First, however, we will consider qualitatively what happens to solid particles flowing vertically upward in turbulent flow in a tube. Of concern is the relative motion of turbulent eddies and the particles.[6]

A particle tends to follow the turbulent air motions if the particle response time[7] to drag forces is small compared to the lifetime of the eddy. In contrast, if the response time is long, the particle will not be appreciably affected by an eddy unless the eddy is large or the time of particle flight through the eddy is long. The effect of the eddies of concern to us for deposition, is the radial motion towards the walls which is imparted to the particles. It is radial motion which eventually causes the particles to impact on the tube walls. In considering this radial motion we must consider that each particle does not move by a continuous radial outward movement. Actually, each particle moves by a series of random outward and inward movements. However, we may consider that on the average there is a net outward radial flux, if all particles in the tube are considered together. These particles will then have a statistically average radial outward movement. The statistical movement must also be considered for the turbulent eddies since eddies are not of a single size but have size and frequency distributions.[8] We do not know whether the average eddy or the eddies at the extreme end of the eddy distribution are the important cause of the radial particle movement. Likewise, for the particle radial velocities, we do not know what portion of the particle velocity distribution is important for causing the radial movement and

final deposition on the tube wall. Obviously, those particles propelled toward the wall at a sufficiently high velocity will have a greater chance of reaching the wall than one caught in a less energetic eddy. Differences also exist between the axial upward movement of the particles and the air.

The relative motion in the axial direction between the particles and the turbulent air is also dependent upon the diffusion time as a particle crosses an eddy and upon the relaxation or response time of a particle. In addition, we will consider the differences in motion due to gravity and the quasi-steady air velocity profile. The quasi-steady air velocity profile is that which would be measured with an air meter with a very slow response time. Thus, a particle in quasi-steady flow with only vertical motion will have a relative motion to the air caused by the gravitational force. A further difference in quasi-steady axial velocities may also occur due to the air velocity profile. To illustrate this difference, we will consider the motion of a particle as it moves from the tube center toward the tube wall in quasi-steady motion. At the tube centerline the axial velocities of both particle and air will be the same except for the gravity effect. This centerline axial velocity for highly turbulent flow will be about 1.2 times the average air velocity across the tube.[9] This means that the situation can occur in which a particle rapidly moves radially from the tube center, and hence, due to inertia, will have a greater local axial velocity than the average air. This difference in axial velocities means that the relative particle residence time in a radially moving eddy may be less than a residence time based on the average axial airflow. Since the residence time may be less, the effect of a radially moving eddy will be less on the radial motion of the example particle.

The high relative axial velocity of the example particle compared to the air velocity must be dissipated as energy; and, hence, particle drag will tend to flatten the air velocity quasi-profile from that air velocity profile for which no particles were present. These differences in air velocity profiles are quantitatively unknown and have been neglected in all deposition models. These differences will be mentioned later in connection with the relative momentum flux-to-the-wall by particle deposition and by turbulent air drag.

To summarize, the description of a particle's inertia and drag in a turbulent flow is more complex than the usual complexities of describing turbulent fluid flow. In turbulent flow, the simplifying assumption is usually made that eddy diffusivities can be used to describe the combined effects of turbulence for fluids. Thus, in a similar simplifying manner, the concepts of turbulent eddy diffusivity of fluid momentum may be extended by analogy to also describe a particle eddy diffusivity. The concept of a particle eddy diffusivity may be questioned, but surely we may define an effective diffusivity in order to write an equation of continuity for particles. To do this, we must assume that the isolated particles in the air can be described by the continuity equation which is a continuous function requiring continuous concentration gradients.

CONTINUITY EQUATION

A continuity equation[10-15] for particles will be written by analogy with the continuity equation for a fluid. The use of this equation is a convenient method by which to ensure that all assumptions are noted in deriving a simple radial diffusive flux equation in a tube. After the general equations are discussed, the simplifications needed to arrive at three deposition models will be discussed. These simplifications are noted since all assumptions have not necessarily been discussed in the derivations of these models of Freidlander and Johnston, Owens, and Davies.

The continuity equation is an analytical expression for the conservation of mass which is

$$\begin{pmatrix}\text{Rate of change}\\ \text{of mass per}\\ \text{unit volume}\end{pmatrix} = \begin{pmatrix}\text{Rate of genera-}\\ \text{tion of mass}\\ \text{per unit volume}\end{pmatrix} - \begin{pmatrix}\text{Flow losses}\\ \text{of mass per}\\ \text{unit volume}\end{pmatrix} - \begin{pmatrix}\text{Non-flow losses}\\ \text{of mass per}\\ \text{unit volume}\end{pmatrix} \quad (1)$$

or analytically in the same order

$$\iiint \frac{dC}{dt}\, dV = \iiint G\, dV - \iint C\, \vec{v} \cdot \vec{n}\, dS - \iint N dS \quad (2)$$

where the integrals are over the volumes, V, and the containing surfaces, S. The variables are the concentration, C; the generation rate, G; (i. e., does a source or sink of material exist within the fluid?); the velocity vector, $\vec{v}$; the outward unit normal through the flow surfaces, $\vec{n}$; and the flux at the solid surfaces, N.

Since we are interested in the steady state deposition of particles in which there is no generation in the air, the term on the left and the first term on the right side of the equation are zero; and thus we have

$$\iint C\vec{v}\cdot\vec{n}\,dS = \iint N dS \quad . \tag{3}$$

The divergence theorem of Gauss[16b] relating the volume integral to the surface integral on the left side of the equation is applied, and thus the equation is changed to the form

$$\iiint \nabla\cdot C\vec{v}\,dV = \iint N dS \quad , \tag{4}$$

where ∇ is the vector differential operator known as "del". For simplicity of discussion this equation will be considered at the present time in a rectangular coordinate system. In rectangular coordinates del reduces to[16d]

$$\nabla = \sum_i \delta_i \frac{\partial}{\partial x_i} \quad , \tag{5}$$

where δ_i are the unit vectors and the x_i are the variables associated with the 1, 2, 3 axes. The divergence term reduces to

$$\nabla\cdot(C\vec{v}) = \sum_i \frac{\partial(C\vec{v})}{\partial x_i} \quad . \tag{6}$$

This means that particle deposition, NdS, is a function of both velocity and concentration profiles.

However, by neglecting the velocity profiles and considering only axial concentration profiles, we can derive an expression used to

to define the experimentally measured deposition velocity, K, in tubes. This deposition velocity is measured by the decrease in average air concentration in a tube. Thus, Equation (4) reduces to

$$AV \nabla C = -N \tag{7}$$

where A is the cross sectional area of the tube of diameter D. V is the average velocity defined by

$$V = \frac{\int_0^{2\pi}\int_0^{D/2} \bar{v}\, r\, dr\, d\theta}{\int_0^{2\pi}\int_0^{D/2} r\, dr\, d\theta} \tag{8}$$

where $\bar{v}$ is the quasi-steady axial velocity which is a function of the tube radius, r, and θ is the angle in cylindrical coordinates.

If Z is the axial coordinate in the vertical tube, then Equation (7) reduces to

$$\frac{\pi D^2}{4} V\, dC = -N\pi D\, dZ \quad . \tag{9}$$

Now the deposition flux, N, is experimentally interpreted to be the product of the deposition velocity and the average concentration:

$$N = K C \quad , \tag{10}$$

where the average concentration is defined by

$$C = \frac{\int_0^{2\pi}\int_0^{D/2} \bar{C}\, r\, dr\, d\theta}{\int_0^{2\pi}\int_0^{D/2} r\, dr\, d\theta} \tag{11}$$

in which $\bar{C}$ is the concentration which is a function of tube radius. Combining Equations (9) and (10) and integrating yields

$$\int_{C_o}^{C} \frac{dC}{C} = -\frac{4}{VD}\int_0^L K\, dZ \quad . \tag{12}$$

Now if K is constant,

$$\ln\left(\frac{C}{C_o}\right) = -4\left(\frac{K}{\bar{V}}\right)\left(\frac{L}{D}\right) \quad . \tag{13}$$

This is the model used to interpret experimental deposition.[1,17,18,19,20,21,22,23] However, we would like to be able to predict deposition from a more fundamental understanding of the particle transport mechanisms. Thus, concepts of particle eddy diffusivity arising from turbulent motion will be considered in relation to the continuity equation.

MOMENTUM FLUX CONCEPTS

We will first consider momentum concepts in rectangular coordinates of a fluid flowing in the x direction with a velocity gradient in the y direction. The shear stress on a surface of constant y is by Newton's law of viscosity,[1]

$$\tau_{xy} = -(\mu + \rho\epsilon)\frac{dy_x}{dy} \tag{14}$$

where μ is the viscosity, ρ is fluid density and ϵ is the eddy diffusivity of the fluid. For turbulent flow, $\rho\epsilon >> \mu$ and, thus, μ is neglected.

Simplifying assumptions can be used to relate the fluid eddy diffusivity to a particle eddy diffusivity;[24,25] this simplifying will be done later. At present, we will consider the momentum flux interpretation of the shear stress. The shear stress, τ_{xy}, may also be interpreted as the flux of x momentum in the y direction.[16a] When deposition occurs on a surface of y = 0, the depositing particles will also contribute to the total momentum flux. The relative contributions to the momentum flux will be considered since we are to use Equation (14) to relate the eddy diffusivity to the shear stress.

The maximum axial momentum associated with particles which deposit on the tube walls will be the product of the particles' mass and the average axial velocity. Now, if the concentration, C, and the deposition velocity, K, are known, we can calculate the momentum flux, τ_p, of particles depositing on the tube wall. In addition, we can compare

the momentum flux, τ_p, of particles to the fluid shear stress, τ_s, at the tube wall by using the definitions of the deposition velocity and the Fanning friction factor, f. The relationship is

$$\frac{\tau_p}{\tau_s} = \frac{K\,C\,m\,V}{f\,\rho\,V^2/2} \tag{15}$$

where m is the particle mass and the areas are comparable tube surface areas. Simplification for spherical particles yields the expression

$$\frac{\tau_p}{\tau_s} = \pi\,\frac{K}{V}\,\frac{C}{f}\,\frac{2}{\rho}\,\frac{d^3\rho_p}{6} \quad . \tag{16}$$

We want to evaluate this equation by using typical values of the constants which would maximize the ratio. These values and a typical concentration are:

$$\begin{aligned} D &= 1 \text{ cm} \\ K/V &= 10^{-2} \\ C &= 1 \text{ particle/cm}^3 \\ f &= 0.003 \\ \rho &= 1 \times 10^{-3} \text{ g/cm}^3 \\ d &= 10\,\mu = 1 \times 10^{-3} \text{ cm} \\ \rho_p &= 1.5 \text{ g/cm}^3 \end{aligned}$$

Evaluation of Equation (16) using these constants suggests that the momentum flux associated with deposition is negligible (10^{-5}) compared to that for fluid shear. This small contribution to the momentum flux tends to indicate that the turbulent air velocity profile may not be significantly affected by the presence of the particles.[26,27] Nevertheless, as the particle approaches the wall from the tube center, the particle axial velocity may be greater than the local air average velocity. The energy of setting air in motion by the particle is neglected.[28]

Thus, our basic assumption is that the particles do not alter the air motion. We next assume that the eddy diffusivity of particles is identical to the eddy diffusivity of the fluid. This assumption is required since we presently have no other recourse, unless we simply say that ϵ_p is a

function of ϵ. Indeed Goldschmidt and Eskinazi[29] have recently shown that, even for mass-mean diameter droplets of only 3 μ, the diffusion of fluid momentum is faster than the diffusion of the droplets. The only other data for turbulent diffusion of particles is that of Wakstein[30] for large 250 μ diam particles in a tube. None of these diffusion data are generally applicable; and hence, we must still assume the equality of diffusion coefficients.

EDDY DIFFUSION COEFFICIENTS

The eddy diffusion coefficient can be calculated from measurements of the turbulent air velocity,

$$v = \bar{v} + v' \tag{17}$$

where the prime denotes the turbulent fluctuations about the average value indicated by the bar notation. For our discussion purposes, we will consider the fluctuation velocities v'_x and v'_y in the x and y directions, respectively. The terms are contained in the x-y component of the momentum flux tensor $\bar{\bar{\tau}}^{(t)}$. (16b) The components of the flux tensor are the Reynolds stresses due to the turbulent fluctuations. The component, τ_{yx}, of the flux tensor is the shear term in the x direction on a plane of constant y. This shear term is the Reynolds stress

$$\tau_{yx} = \rho \overline{v'_x v'_y} \quad , \tag{18}$$

and contains the product of the fluctuation velocities v'_x and v'_y in the direction of, and perpendicular to, the main flow. The bar over the product denotes the time average of the product. By combining Equations (14 and 18), the eddy diffusion coefficient is defined as

$$\epsilon = \frac{\overline{v'_x v'_y}}{\overline{\frac{dv_x}{dy}}} \quad . \tag{19}$$

This value of ϵ is not constant and increases as the distance from the wall is increased.

To be noted is the implicit assumption that an eddy diffusion coefficient has meaning. For instance, another relationship between Reynolds

stresses and velocity gradients is von Karman's similarity hypothesis[16c] which for a plane is

$$\tau_{yx} = -\rho\varkappa^2 \left| \frac{(d\bar{v}_x/dy)^3}{(d^2\bar{v}_x/d_y^{\,2})^2} \right| \frac{d\bar{v}_x}{dy} \tag{20}$$

were $\varkappa$ is a "universal" constant. As seen, in comparison with Equation (14), an eddy diffusivity does not appear in the equation. Similarly, for axial tube flow,

$$\tau_{rz} = -\rho\varkappa^2 \left| \frac{\left(\frac{d\bar{v}_z}{dr}\right)^3}{\left(\frac{d^2\bar{v}_z}{dr^2} - \frac{1}{r}\frac{d\bar{v}_z}{dr}\right)^2} \right| \frac{d\bar{v}_z}{dr} \quad . \tag{21}$$

For cylindrical coordinates, an added term is required in the denominator.

CONCENTRATION DISTRIBUTION IN TURBULENT FLOW

We have now looked at the evaluation of eddy diffusion coefficients, and also the continuity equation based on quasi-steady flow velocity. These will now be combined for turbulent flow. In turbulent flow the concentration and velocity may be represented by

$$C = \bar{C} + C' \tag{22}$$

and

$$v = \bar{v} + v' \tag{23}$$

where the prime signifies the turbulent fluctuations about the average value indicated by the bar notation. These values are substituted into the continuity equation

$$\frac{\partial C}{\partial t} = -\nabla\cdot(Cv) + D\nabla^2 C \tag{24}$$

where D is the diffusivity in order to obtain the time smoothed equation of continuity

$$\frac{\partial \bar{C}}{\partial t} = -\nabla\cdot(\overline{vC}) - \nabla\cdot\overline{v'C'} + D\nabla^2 C \quad . \tag{25}$$

In this time-smoothed equation the product of a bar term times a primed term was zero, since the integral over time of the primed term is zero. Since the substantial time derivative is defined as

$$\frac{DC}{Dt} = -\frac{\partial C}{\partial t} + \bar{v}\cdot\nabla\bar{C} \quad , \tag{26}$$

and

$$\nabla\bar{v} = 0 \tag{27}$$

for an incompressible fluid, Equation (25) can be expressed in terms of laminar and turbulent diffusion fluxes

$$\frac{DC}{Dt} = -(\nabla\cdot\bar{J}^{(\ell)}) - (\nabla\cdot\bar{J}^{(t)}) \tag{28}$$

which describes the substantial time derivative following the $\bar{v}$ motion of the particles. This form of the equation readily shows that the concentration change on the left side of the equation is caused by the divergence on the right side of the equation of the laminar and the turbulent diffusion fluxes, respectively. The laminar flux is relatively unimportant, except possibly in the final approach to deposition on a wall surface. Even here, a mechanisms of particle motion by free flight would appear to be more significant than diffusion. Thus, laminar diffusion will be assumed negligible in subsequent discussions. The turbulent diffusion flux is from Equations (25) and (28),

$$\bar{J}_i^{(t)} = \overline{v_i'C'} \quad , \tag{29}$$

and by analogy with Flick's law of diffusion, we write

$$\bar{J}_y^{(t)} = -\varepsilon_\rho \frac{dC}{dy} \quad . \tag{30}$$

This is the point at which we apply our assumption of equality of the eddy diffusivities,

$$\varepsilon_\rho = \varepsilon \quad . \tag{31}$$

Equation (25) now becomes

$$\frac{\partial \bar{C}}{\partial t} = -\nabla\cdot(\overline{vC}) - \nabla\cdot(\epsilon \nabla \bar{C}) \quad . \tag{32}$$

We simplify the equation by setting the time derivative equal to zero by observing the concentration at a fixed location at steady flow. Thus,

$$\nabla\cdot(\overline{vC}) = -\nabla\cdot(\epsilon\nabla\bar{C}) \quad . \tag{33}$$

We now assume axial symmetry in a vertical tube, diffusion only in the radial direction, and quasi-steady flow only in the axial direction. With these assumptions the equation reduces to

$$rv_z \frac{\partial C}{\partial Z} + \underline{\frac{\partial}{\partial r}(Crv_r)} = -\frac{\partial}{\partial r}(\epsilon r \frac{\partial C}{\partial r}) \quad . \tag{34}$$

The underlined term is also zero under our assumptions since

$$v_r = 0 \quad . \tag{35}$$

This underlined term is a source of criticism of the existing models of deposition of Friedlander and Johnstone, Owen, and Davies. In their models the assumption is made that particles diffuse up to near a deposition surface. The last stage of deposition is by a "free-flight" in which the particles are deposited in a projectile-like manner. The free-flight distance, S,

$$S = \tau v_r \quad . \tag{36}$$

where the relaxation time, τ, for a spherical particle is

$$\tau = \frac{\rho_p d^2}{18\mu} \quad . \tag{37}$$

The radial velocity, v_r, is assumed to be acquired at the last instant of the diffusion before free-flight occurs. This is an unrealistic assumption in terms of the continuity equation, since an instantaneous source of velocity is not present only at the distance S for each particle. We could consider that no radial velocity exists and from Equation (34), after dropping the term containing v_r, define an eddy diffusivity by

$$\epsilon = \frac{\int_0^r r\, v_z \frac{\partial C}{\partial r}\, dr}{r \frac{\partial C}{\partial r}} \quad . \tag{38}$$

However, evaluation of this equation would require a detailed knowledge of the concentration profiles. If a source of radial velocity did exist at the distance S, other sources of radial velocity should also be present throughout the tube. However, particle radial velocity data are not known.

Thus, we too, resort to the assumption that the radial velocity is zero. Integration of Equation (34) yields

$$\int_0^R r\, v_z \frac{\partial C}{\partial Z}\, dr = 2\pi \epsilon\, r \frac{\partial C}{\partial r}\bigg|_{r=R} \tag{39}$$

$$= N$$

where N is the experimental total deposition at steady state. This is the equation to which the models of Friedlander and Johnstone, Owen, and Davies will be compared.

MODEL REVIEW

All three models predict deposition velocities and are discussed and evaluated in terms of deposition in a two-dimensional rectangular coordinate system. The airflow is in the x direction and deposition is in the y direction. The conceptual bases of Friedlander and Johnstone, and Owen models are similar; that is, a boundary layer exists between a deposition surface and a central core of uniform concentration. Particle motion is by eddy diffusion from the uniform core to within a free flight distance of the deposition surface. In comparison to a uniform core, in Davies model particle motion is by eddy diffusion from the tube center to the free-flight distance. The free-flight distance is hypothetical, but is a useful concept for modeling. At the free-flight distance, particles have a sufficient velocity toward a surface to oppose viscous drag and to cause the particles to deposit on the surface.

The rationale behind the assumption of a free-flight distance is most readily seen, if we consider particle deposition on the underside of a horizontal surface. For this geometry the forces on particles are turbulent diffusion forces in the upward direction which are opposed by gravitational force. Owen illustrates that the gravitational force may very well be much greater than the diffusional force. However, we have all seen where dust has collected on the underside of an objective. This means that particles must have had a finite velocity which caused the particles to impact. All three writers agree that this velocity must exist, but are in serious disagreement as to what velocity is best.

Each model will be discussed, but first we will define dimensionless terms which are used in each model. A dimensionless distance is

$$y^+ = y \frac{u_*}{\nu} \tag{40}$$

and a dimensionless velocity is

$$u^+ = u/u_* \tag{41}$$

where u_* is the friction velocity and ν is the kinematic viscosity. The friction velocity is defined as

$$u_* = \left(\frac{\tau_o}{\rho}\right)^{1/2} \tag{42}$$

where τ_o is the wall shear stress. If τ_o is not known, it can be calculated from pressure drop data in a tube or from correlations of the Fanning friction factor, f. For turbulent flow in tubes,

$$2\pi R \tau_o = \pi R^2 \frac{dp}{dx} \tag{43}$$

where R is the tube radius and dp/dx is the pressure drop. Thus,

$$\tau_o = \frac{R}{2} \frac{dp}{dx} \tag{44}$$

and the friction velocity is

$$u_* = \left(\frac{R}{2\rho}\frac{dp}{dx}\right)^{1/2} \quad . \tag{45}$$

Similarly,

$$\tau_o = f\,\rho\,\frac{V^2}{2} \tag{46}$$

and combining Equations (42) and (46) yields the equality

$$u_* = \left(\frac{\tau_o}{\rho}\right)^{1/2} = V\left(\frac{f}{2}\right)^{1/2} \quad . \tag{47}$$

The boundary layer is usually described in terms of the distance, y^+, from the surface. In a structuring of the boundary layer, the region below a y^+ of 5 is considered the laminar sublayer. The region between y^+ of 5 and about 30 is the buffer layer. The region beyond a y^+ of 30 is in the turbulent core.

MODEL OF FRIEDLANDER AND JOHNSTONE

The structural layer concept of the boundary layer was used by Friedlander and Johnstone to predict deposition velocities from the one-dimensional model

$$N = -\epsilon\frac{dC}{dy} \quad . \tag{48}$$

This equation was converted to dimensionless distances indicated by a superscript of plus and then integrated

$$\int_0^{C_s} dC = -\frac{\nu N}{u_*}\int_{S^+}^{5}\frac{dy^+}{\epsilon} \tag{49}$$

where u_* is the friction velocity and S is the particle stop distance given in dimensionless form, S^+, by

$$S^+ = S\frac{u_*}{\nu} = \frac{\rho d^2 V_o u_*}{18\mu\nu} \quad . \tag{50}$$

This stop distance is calculated on a basis of a single constant value for the velocity of approaching the wall. The velocity is

$$V_o = 0.9\, u_* = 0.9\sqrt{f/2}\, V \qquad (51)$$

for all particles. Particle inertia resulting from this velocity is assumed to deposit the particle.

Equation (48) is also integrated in the buffer layer with integration constants to cause identical concentration at the meeting of the two layers. In the outer turbulent core the Reynolds analogy was used to determine the concentration. However, the buffer-core interface concentrations were not identical as calculated from the buffer layer and turbulent core equations. The three equations were combined to predict the deposition velocity, K, as a function of V, f, and S^+. The predicted values agree reasonably well with their experimental results.

The experiments were performed by sizing and counting the particles deposited on a tube wall and comparing them with particles which were not deposited. Similar experiments were performed by Postma and Schwendiman[31] who compared their experimental results with those predicted from the equations of Friedlander and Johnstone.[1] The data show a general grouping around the predicted values when K/V is plotted versus S^+. This empirical correlation was used by Sehmel and Schwendiman[21] to predict the deposition behavior of a polydispersed aerosol. Reasonable experimental agreement was found for other than re-entrainment conditions.

MODEL OF OWEN

Owen[2] in his model is the only one of the three who puts in a factor for the difference between a particle diffusivity and the diffusivity of momentum. Equation (48) was also integrated by Owen who considered diffusion from a uniform core to a distance from the surface. This distance corresponds to a free-flight distance over which the final stage of deposition occurred. The final equation for predicting the deposition velocity was independent of particle size. This is in disagreement with experimental deposition velocities in tubes.

MODEL OF DAVIES

Davies[3, 4, 5] also uses turbulent diffusivities to calculate the deposition velocity. He presents a correlation for turbulent diffusivities

$$\frac{\epsilon}{\nu} = \frac{(y^+)^{(4 - y^{+0.08})}}{1000\left(\frac{2.5 \times 10^7}{Re}\right)^{\left(\frac{y^+}{400 + y^+}\right)}} \qquad (52)$$

using the data of Lin and Moulton,[32] Laufer,[33] Owen,[2] and Schlinger and Sage.[34] This correlation is then used to calculate diffusion up to the free-flight distance. The diffusion calculations are made for diffusion in a rectangular coordinate system and the results applied to the cylindrical coordinate system of tubes. The diffusion equation in the rectangular coordinate system is integrated from a distance, y^+, from the surface to a distance, R^+, which corresponds to a tube diameter. This particular y^+ depends upon particle size and is evaluated by a simultaneous equality of solution of the stop distance and the fluctuating velocity, v', at y^+. Tabulated values are shown for the calculation of the deposition velocity.

We have now written the general equations of continuity for particles and discussed some of the complicating factors and the assumptions required. Next we briefly reviewed three deposition models in light of our general discussion. As we have seen, each model has at least one assumption which could be improved upon. What, then, do we suggest as an improved theoretical model to predict deposition velocities?

It is proposed that the cylindrical coordinate diffusion equation,

$$2\pi r \epsilon \frac{\partial C}{\partial r} = N \qquad (53)$$

with the constant total flux, N, at r, be integrated in the cylindrical coordinate system. The eddy diffusivity can be calculated from a similar correlation procedure as used by Davies.

Similar to Davies' calculation for rectangular coordinates, the model will yield the total wall flux. The final approach to the wall will be calculated on the basis that the particle inertia will be due to the root mean square radial velocity of the air located at the start of a projectile-like motion. These velocities are much less than the velocity used by Friedlander and Johnstone which is a velocity characteristic of a much greater distance from

the tube wall. After a deposition, N, per unit area, is calculated, the deposition velocity will be calculated from the equation

$$K = \frac{N}{\bar{C}} = \frac{N}{\left[\frac{\int_0^R rC\,dr}{\int_0^R r\,dr}\right]} \qquad (54)$$

where the upper limit of integration is actually R minus the free-flight distance. This upper limit is used for ease of calculations and has a negligible effect upon C. The initial calculated results from this model will be discussed later in a comparison of experimental results with theoretical predictions.

EXPERIMENTAL

The experimental deposition apparatus is shown schematically in Figure 1. Particles of either uranine or uranine-methylene blue were generated in a narrow size range using the spinning disc generator. The particles have a density of 1.5 g/cm^3.[35] These particles were passed into a 50 gal holding chamber. The holding chamber had three exit ports from which the particles were passed vertically upward through aluminum tubes which served as deposition test sections, were sampled to determine particle size, or were exhausted into a high efficiency filter. The test sections were up to 50 ft long and the nominal inside diameters were 0.21, 0.62, 1.152, and 2.81 in. Either a single test section or two parallel test sections were used to simultaneously determine the deposition. To begin an experiment the tubes were first washed, rinsed with distilled water, and then supported at several locations along the length of the test section. Each test section was made up of individual tubes up to 12 ft in length. These individual tubes were held together by butting the ends within a sheet of shim stock. A tight-fitting rubber tubing was slipped over the shim stock and then the rubber tubing sealed with tape to the aluminum tubing. This procedure aligned the tubes and formed a tight-fitting joint. The weight of the tubes helped to hold the tubes together.

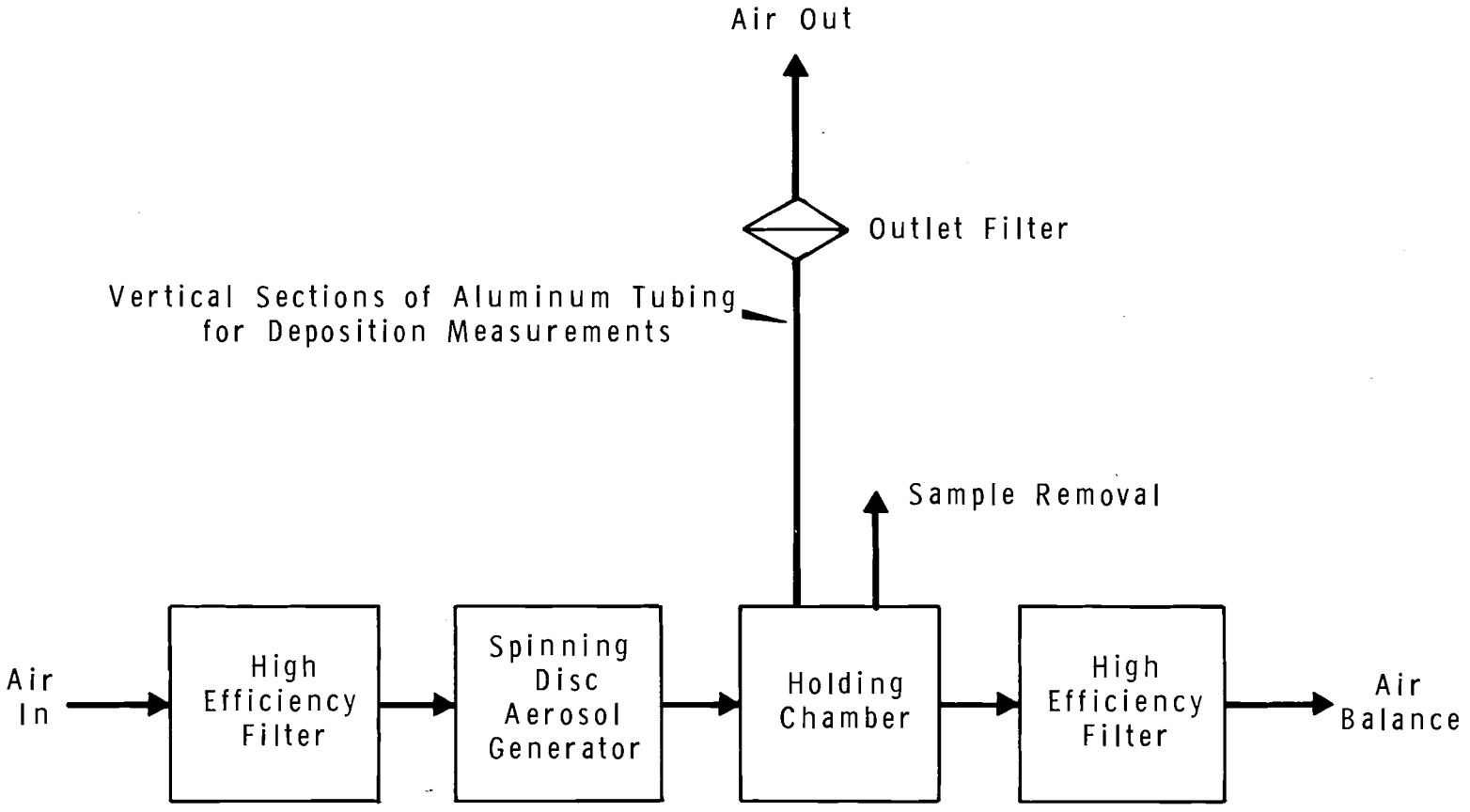

Neg 0672177-4

FIGURE 1. Schematic Diagram Showing the Deposition Apparatus

To evaluate deposition, a mass balance of particle deposition was made from fluorimetric analyses of system washings. The deposition on tubes was measured either by washing the entire length of tubing or by cutting the tubing into lengths as short as 1 in. and then washing each short length. The total mass passing through the tubes was washed from the filter and filter holder. The distilled water wash liquid was analyzed in a fluorimeter using a narrow pass filter which peaks at 360 mμ and for the secondary a narrow pass filter which peaks at 546 mμ.

In some cases, the tubes were purposely made tacky to simulate a perfect particle sink. To form the tacky coating, the end of the tube was first filled with petroleum jelly. The tubing was then heated with an air heater. The tube was rotated as the petroleum jelly melted and slid down the tube. This procedure covered the wall with a tacky coating. Additional heating of the tube thinned and smoothed the coating.

In addition to deposition data, the axial flux of particles was determined as a function of radius in a 2.81 in. ID tube. The experimental arrangement consisted of a filter placed completely across the tube. The axial flux of particles was determined from fluorimetric analysis of filter sections. To determine the filter collection profiles, monodispersed uranine particles were passed upwards through the 2.81 in. ID aluminum tube. The filter was located at the 24 ft level at a slipjoint in the tubing. Within the joint was a tight fitting wire screen which served as a backing for the filter. The screen was fastened with a silicone rubber to the tube wall. The filter was placed across the screen and then the tubes were pressed firmly together. The inner shoulder of the slipjoint pressed against the filter, which in turn pressed against the silicone rubber. The seal was positive since the seal region was devoid of particles after particles had been collected. Also, the slipjoint was sealed with tape to assure noninleakage.

After particle collection, each filter was cut into concentric annuli for fluorimetric analysis to determine the filter loading. Initially, the filter was cut consecutively with cork borers into five sections, but

subsequently, the filter was cut simultaneously into six sections. The inside diameters of the cutting edge are given in Table I.

TABLE I. Filter Section Dimensions

Cutting Edge Diameters, in.	
Consecutive Cuts	Simultaneous Cuts
0.426	0.427
0.926	0.927
1.444	1.438
1.932	1.926
2.318	2.313
	2.600

RESULTS AND DISCUSSION

The deposition data are reported as deposition velocities as a function of Reynolds number and particle size for each tube diameter in Figures 2 through 5. The deposition velocities range from about 10^{-4} to 10 cm/sec. The solid curves are for each particle size, and these curves are intercepted by broken line curves which show the calculated percent deposition within a 10 ft length of vertical tubing. These figures will be discussed after the calculations and several deposition effects are discussed.

CALCULATION OF DEPOSITION VELOCITIES

The deposition velocities are calculated from the average particle concentration decrease in the tube as a function of distance along the tube length. Since the concentration is directly proportional to the mass of particles, the deposition velocities can also be calculated from the average mass decrease in the tube as a function of distance along the tube length. Thus, in the actual calculations, the total mass of particles is used. The total mass is obtained by tabulating the cumulative amount measured as a function of distance starting at the outlet filter. These cumulative amounts are normalized to the amount entering the inlet of any tube length of interest.

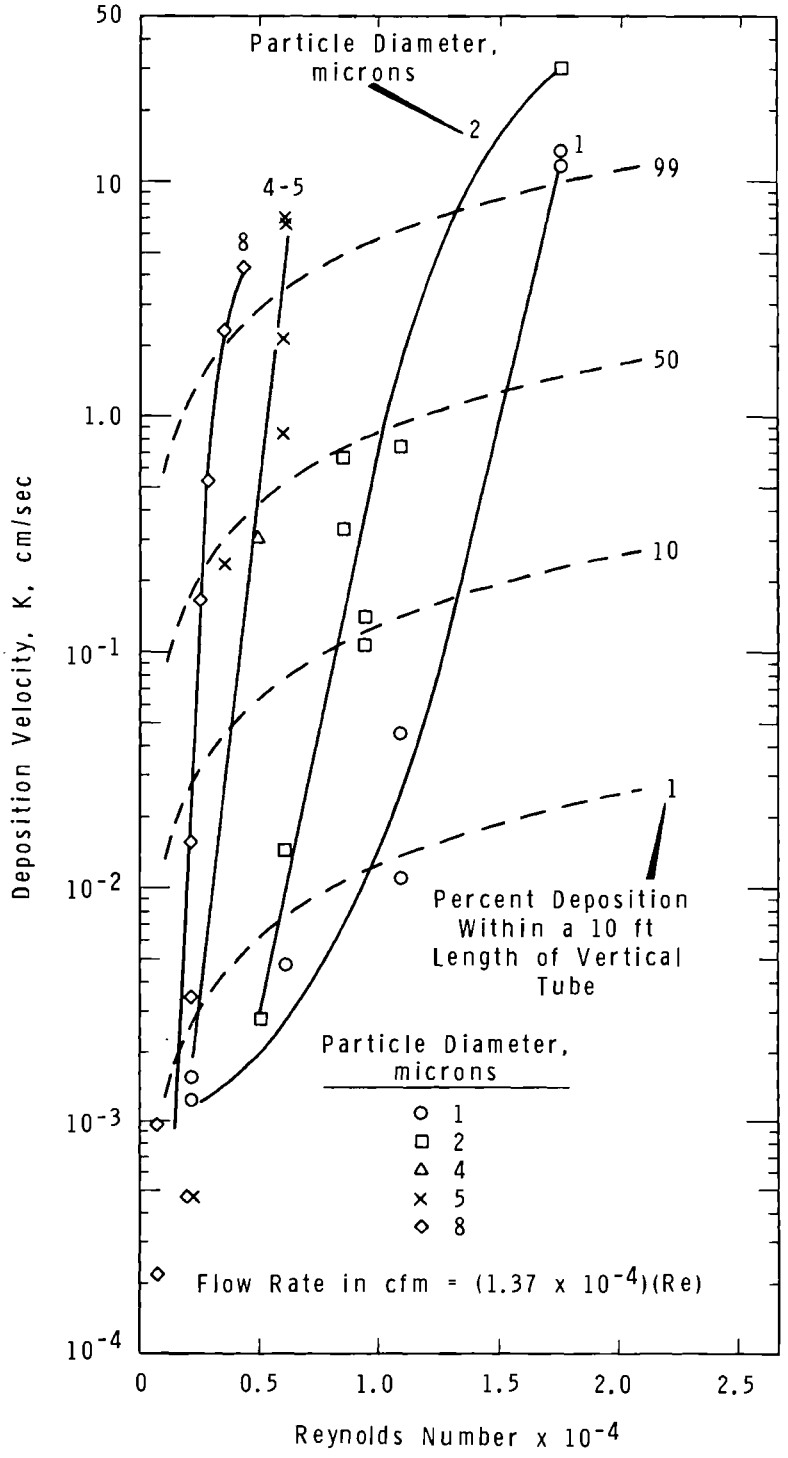

Neg 0673032-1

FIGURE 2. Deposition as a Function of Reynolds Number for Methylene Blue-Uranine Particles in 0.21 in. ID Tubes

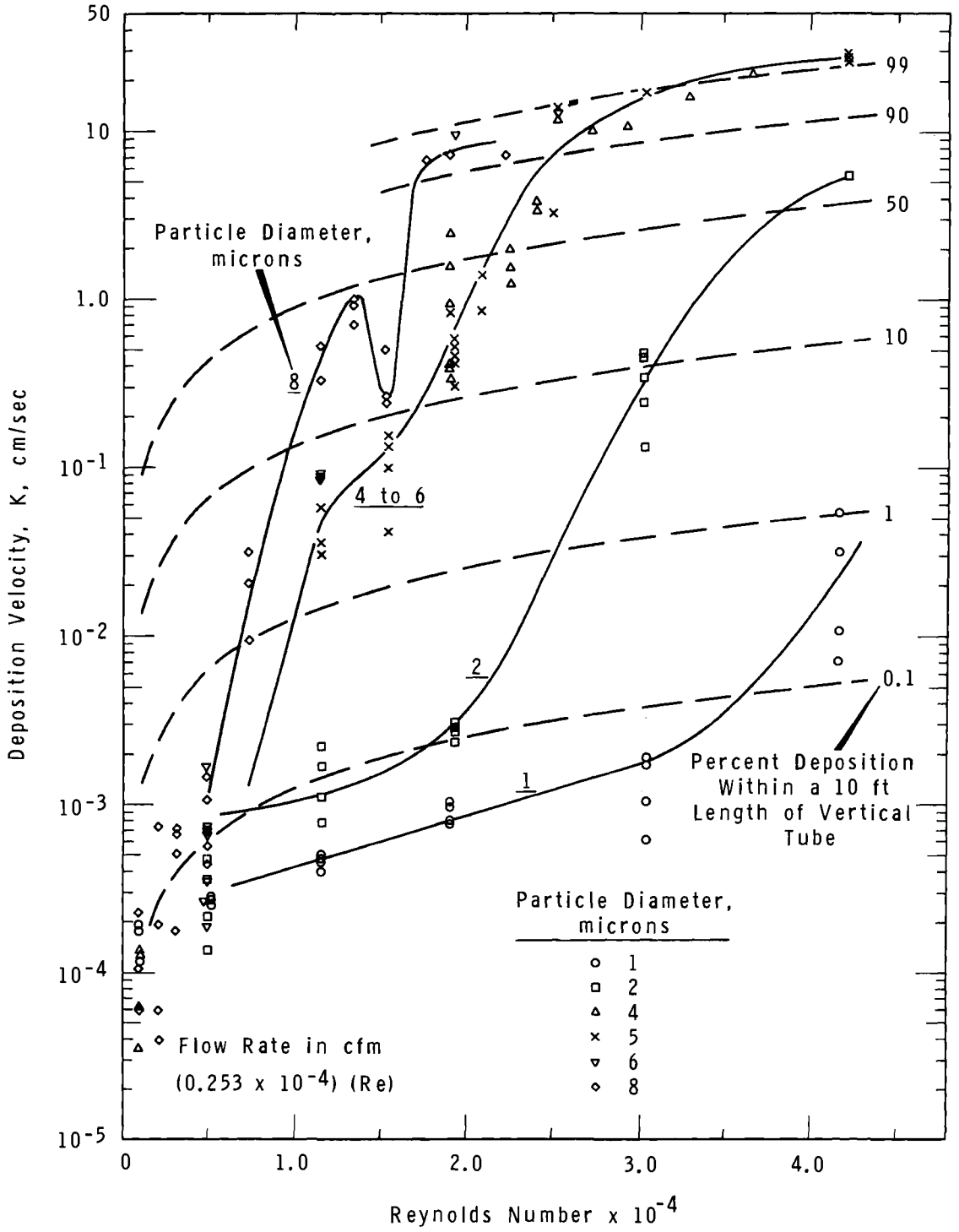

Neg 0672177-8

FIGURE 3. Deposition as a Function of Reynolds Number for Methylene Blue-Uranine Particles in 0.62 in. ID Tubes

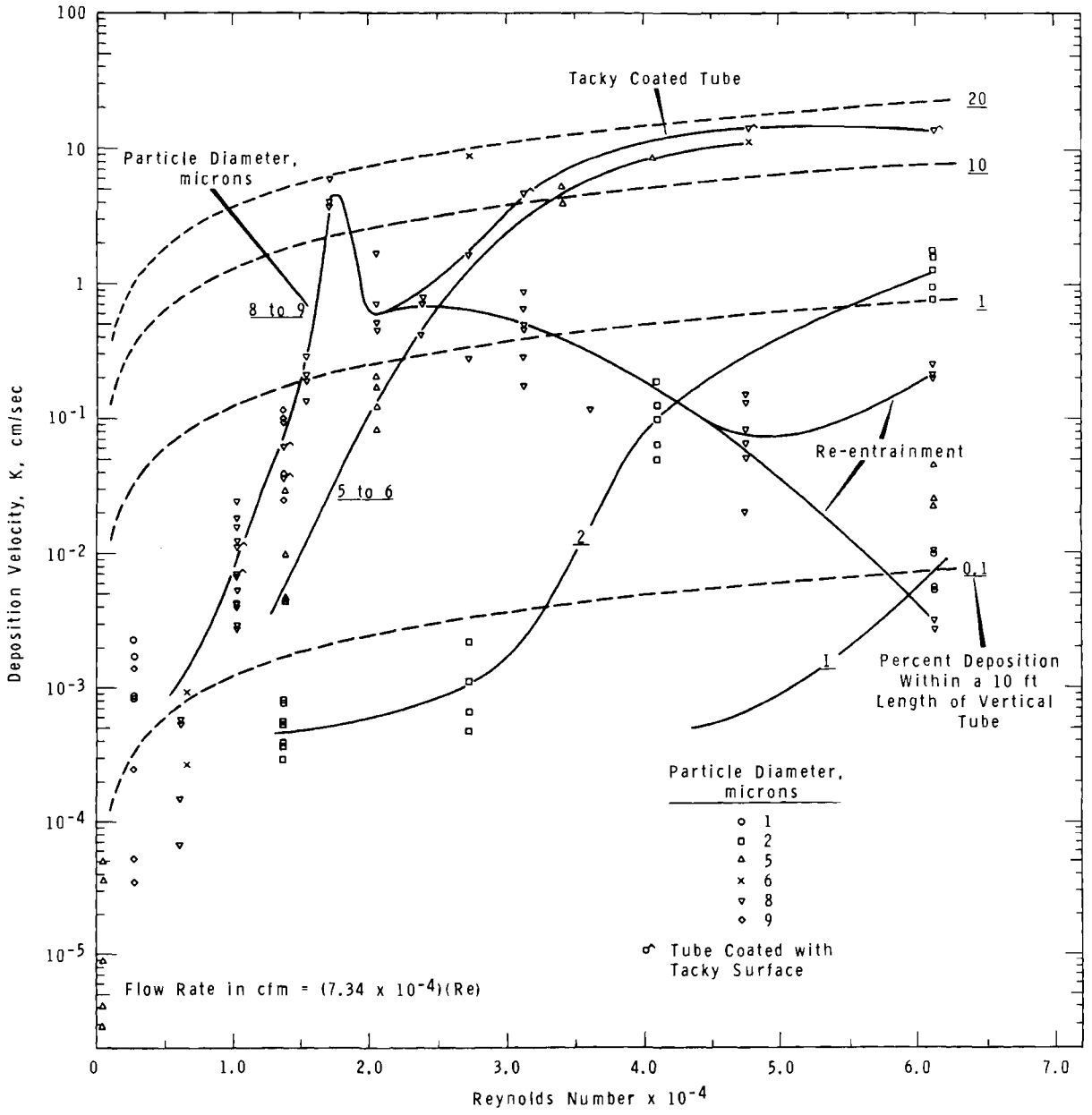

Neg 0673032-2

FIGURE 4. Deposition as a Function of Air Flow Rate for Methylene Blue-Uranine Particles in 1. 152 in. ID Tubes

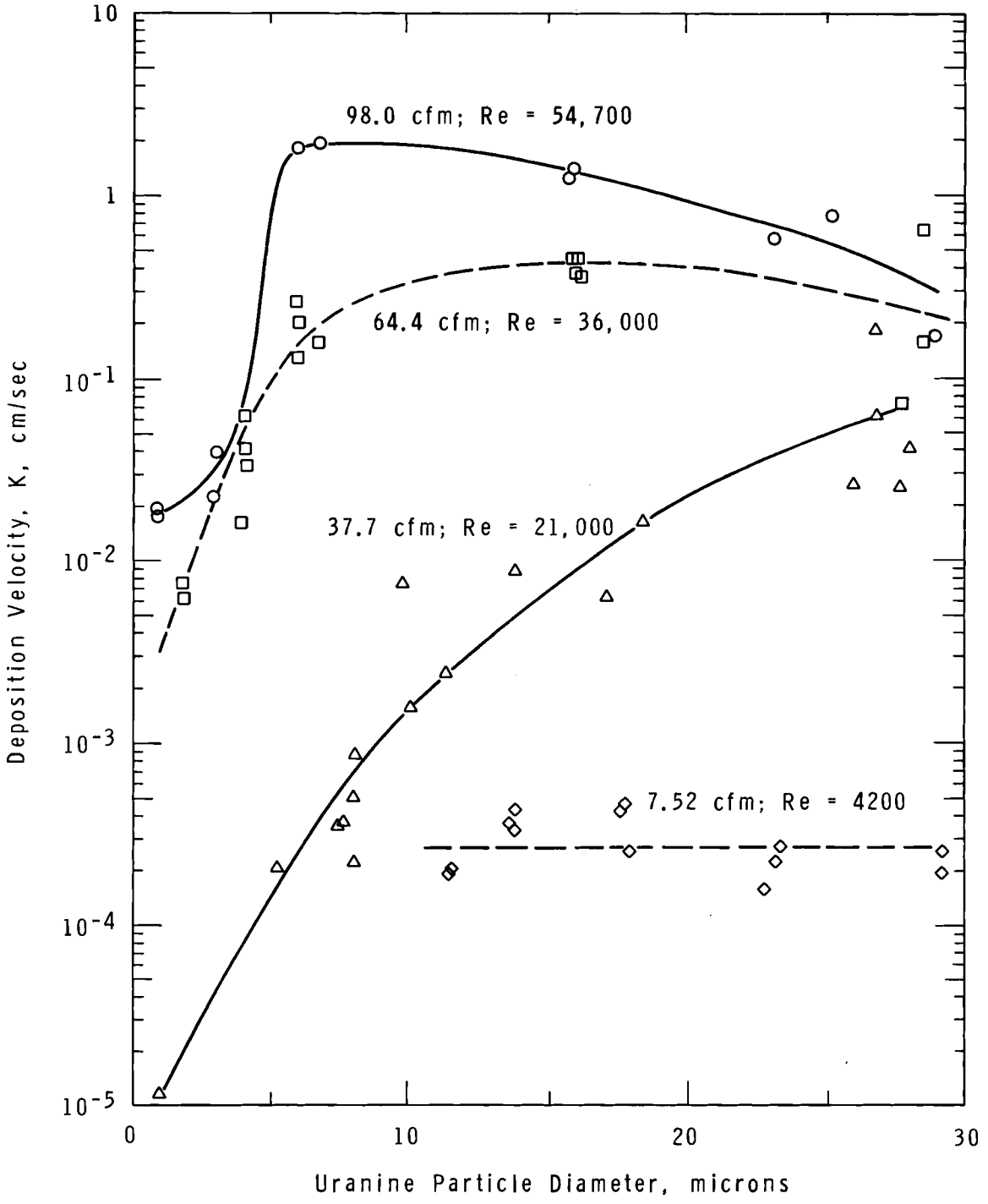

Neg 0674029-10

FIGURE 5. Effect of Reynolds Number on the Deposition Velocity of Particles Within 2.81 in. ID Vertical Tubes

Illustrative examples of these profiles will be discussed later; but first, we will look at the equations we use for calculating the deposition velocity from the measured axial concentration profile. The deposition velocity is calculated from

$$K = -\left(\ln \frac{C}{C_o}\right)\left(\frac{V}{4}\frac{D}{L}\right) \tag{55}$$

which is obtained from Equation (13). For graphical evaluation of the deposition velocity the logarithm of the normalized concentration, C/C_o, is plotted as a linear function of the distance from the inlet on semilog paper. The slope is $(-\frac{4K}{DV})$.

For low deposition rates, graphical evaluation of the deposition velocity through the use of seimlog paper is impractical since the slope cannot be obtained graphically. In this case, we use the first term of the power series expansion of the log function. This then yields the expression

$$\frac{K}{V} = -\left(\frac{\Delta C}{C_o}\right)\left(\frac{1}{4}\frac{D}{L}\right) \tag{56}$$

in which ΔC is the concentration drop below C_o at the distance L from the inlet. This means that cumulative deposition is a linear function of cumulative distance. Of more interest is the concentration versus distance. In this case Equation (56) is rearranged to yield

$$\frac{K}{V} = -\left(1 - \frac{C}{C_o}\right)\left(\frac{1}{4}\frac{D}{L}\right) \tag{57}$$

or

$$\frac{C}{C_o} = 1 - 4\left(\frac{K}{V}\right)\left(\frac{L}{D}\right) \quad . \tag{58}$$

Thus, a plot of the normalized concentration versus cumulative distance has a slope of $[-4K/(VD)]$ on rectangular coordinate paper. Since the velocity, V, and the tube diameter, D, are known, the deposition velocity can be calculated from the slope. The slope was not always constant--in some cases

distinct curvature was observed. For cases of limited curvature a straight line was assumed to represent the data. Also, sometimes the air concentration decreased linearly at two slopes for two portions of the plot for a single deposition experiment. In this case two deposition velocities are reported. At other times, as for some re-entrainment conditions or for polydispersed particles, the profiles were also nonlinear. In these cases, a single deposition velocity cannot be calculated. Illustrative profiles will be discussed which show linear profiles, nonlinear profiles, joint effects, and end effects.

AXIAL CONCENTRATION PROFILES

The axial decrease in the average air concentration of particles as a function of tube length is termed the concentration profile. Concentration profiles for a 48 ft length of 0.62 in. ID tubing are shown in Figure 6 for a Reynolds number of 19,000. The curved profile shows the presence of some small satellite particles. On the semilog coordinates, we see that the concentration profile is linear as the normalized concentration decreases to 10% within the first 8 ft. This linearity is as expected for single-sized particles. Between 8 to 24 ft, the profile shows curvature, and beyond 24 ft the normalized concentration tends to remain constant at about 2%. This 2% remaining airborne is attributed to "satellite" particles[36] which are formed just after the primary particles leave the edge of the spinning disc in the aerosol generator. Most of these satellites are removed in the generator, but some remain as seen from the leveling to 2% of the concentration profile. These satellites are of the order of 1 μ in comparison to the 9 μ diam of the primary particle size. Since these satellite particles do not deposit to any significant extent for the flow rate and tube diameter used, we simply subtract out the 2% concentration of the satellite particles from the measured profile. In this case, we get a linear profile characteristic of the 9 μ particles. The concentration of 9 μ particles is seen to decrease to 1% in only 15 ft. The deposition velocity for 9 μ particles is calculated from the slope of this linear profile.

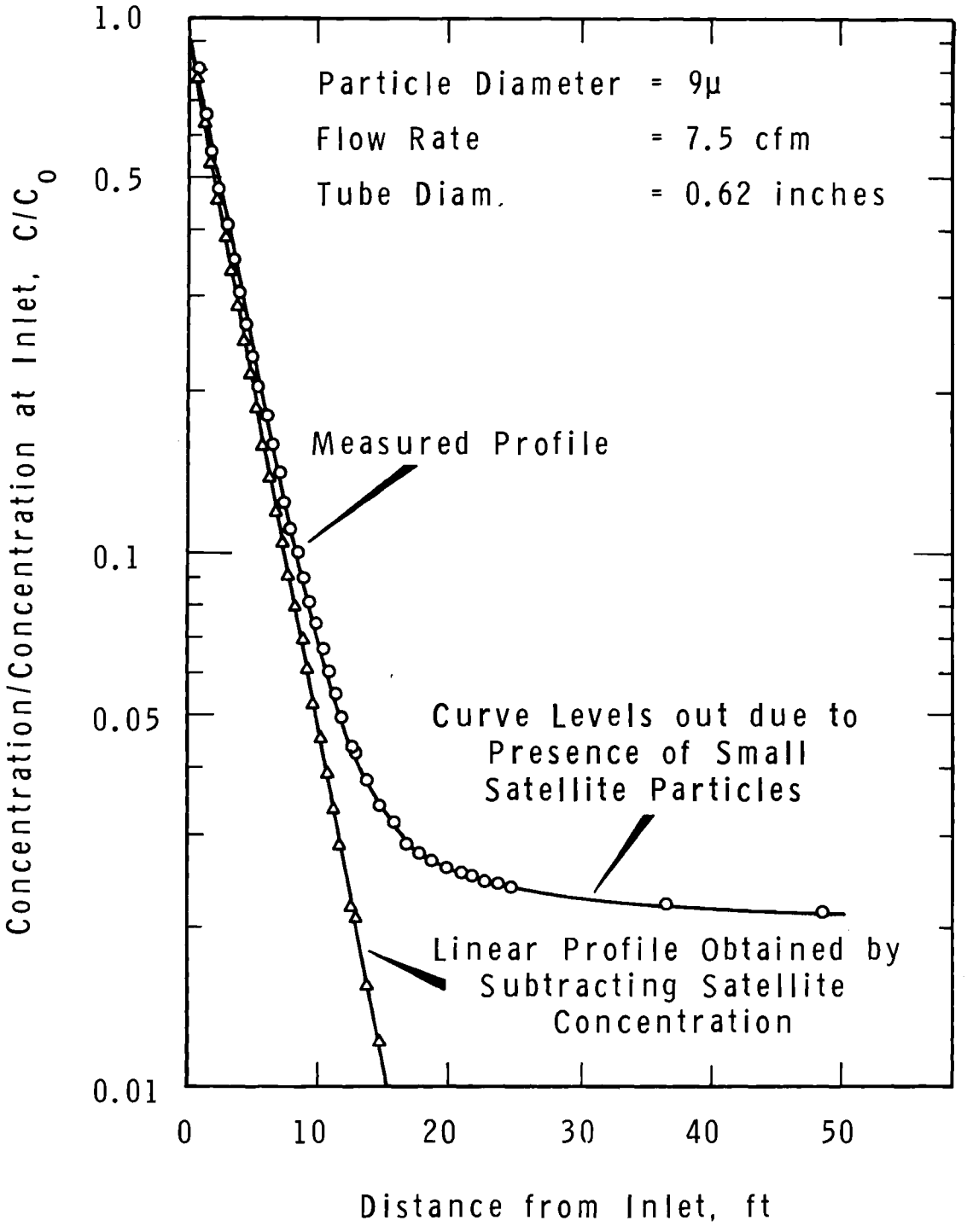

Neg 0673004

FIGURE 6. Aerosol Concentration Profile Showing the Effect of Sattellite Particles

The measured profile is also useful to illustrate the experimental method of sectioning the tubes. For the first 12 ft, the tube was sectioned into 6 in. lengths. For the next 12 ft, the tube was cut into 1 ft lengths. The decision for the length of each section was based upon determining profile curvature or longer lengths to determine a significant deposition, if deposition were low. Short lengths were also used to establish the extent of end and internal effects.

END AND INTERNAL EFFECTS

End and internal effects as well as deposition differences between individual 12 ft tube lengths will be discussed in terms of profiles illustrated in Figure 7. These data were obtained in a single experiment in which tubes were used for two parallel deposition measurements. Particles were introduced into the holding chamber and were simultaneously withdrawn vertically upward through two separate deposition tubes. The profiles shown are from the second 12 ft length of individual tubing in each parallel tube. The tube inlets were at the same height, and the fractional deposition in each tube before the tube inlets were comparable. The flow rates were within 2% of one another as confirmed by the total mass of particles entering from the holding chamber into the two parallel sections.

The first point to note is that the total deposition in one 12 ft length was 2% and in the other was 21%. In comparison to other duplicates for these conditions, the 21% is the expected value. What then is the cause for only a 2% deposition?

In Figure 7, the two profiles are identified with either "smooth" or "rough" surfaced tubes. Smooth or rough represent only a qualitative visual estimate, as the aluminum tubes were too soft for actual surface roughness measurement with the profilometer available. After obtaining these concentration profiles, we tried to obtain the same wide variation in the deposition by purposely choosing the smoothest and roughest available as-received tubes. However, both these chosen tubes showed identical deposition, which appears to rule out the influence on deposition of surface roughness within the range of commercial tube quality. It should be mentioned that the experimental conditions are those for which re-entrainment

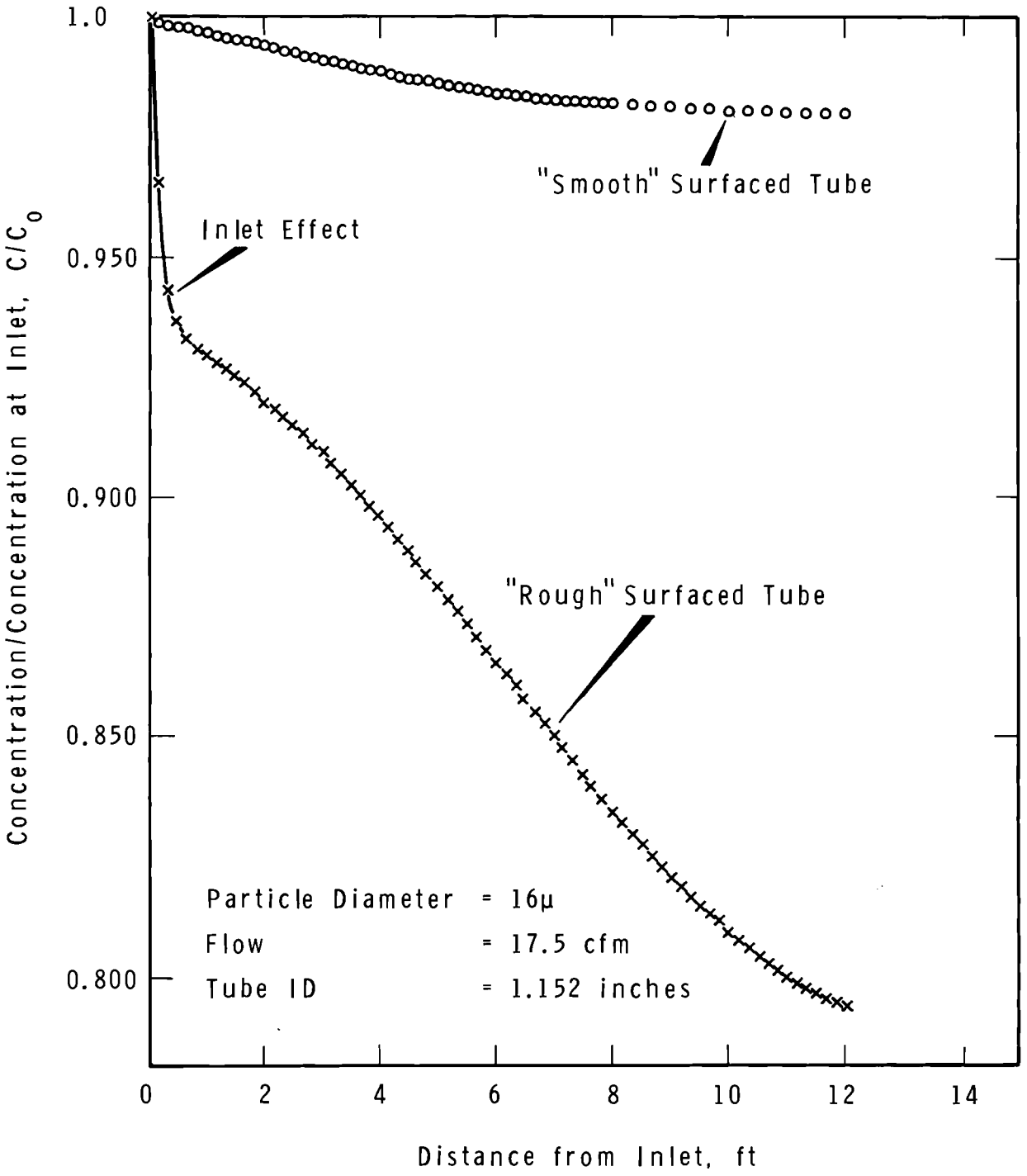

Neg 0672863-2

FIGURE 7. Aerosol Concentration Profiles Showing the Effect of Tube Roughness on Deposition for Re-Entrainment Conditions

occurs and [37, 38] thus subtle differences in surface quality may be more important than for the case where deposition occurs without re-entrainment. The 2% deposition must be considered anomalous at present. If the conditions causing the anomoly could be identified, the conditions might be utilized to minimize deposition in practical situations.

A second point to be noted from the figure is the two linear profiles for the "smooth" surfaced tube. These profiles change between 6 to 7 ft from the inlet. The slope decreases by a factor of four which means that the deposition velocity also changes by a factor of four. Possible causes of the slope change include vibration, since only the tube ends were supported. However, the change of slope is not apparent for the "rough" tube which was similarly supported. Also, in other measurements, the tubes have been supported at various locations. None of these locations has produced a consistent change in deposition. None of the possibilities has been consistently proven; and, hence, we do not have an explanation of the changes in internal deposition as indicated by the two slopes.

A third point to note from this figure is the inlet effect shown for the "rough" surfaced tube. The deposition is relatively high for the first 6 in. of the tube. Similarly, in the eleventh foot, a minor outlet effect is indicated but not labeled. In general, the inlet effect is usually greater than the outlet effect. However, neither may be important as seen for the profile for the "smooth" surfaced tube. To be emphasized is that these inlet and outlet effects as described are associated with tubes which are connected to similar sized tubes. The similar sized tubes were of sufficient length to minimize any end effects associated with rapid contraction or expansion of the test sections.

The deposition velocities are calculated from the profiles by neglecting the end effects. However, if the entire tube were washed as a single unit when deposition was low, the calculated deposition velocities would also include the end effects. Joint effects also exist in addition to end and internal effects.

JOINT EFFECTS

We have noted that significant differences in deposition rate may occur at joints, even though they are designed to minimize wall discontinuities. As described earlier, the tube joints were held within a shim stock sleeve over which was placed rubber tubing effectively aligning the tubes. In Figure 8 are shown the effects of a tube joint at 6 ft. Beyond 6 ft the slope decreases by about 25%. These two tubes, as previously mentioned, were chosen by visual inspection to the smoothest and roughest available from about twelve as-received tubes. Each 12 ft tube was cut into two, 6 ft lengths. These were put into parallel sections so that a 6 ft length from each 12 ft length was in each deposition section. The tube placement was such that a smooth and a rough tube were to be compared at each height. As seen from the figure, the deposition was the same for tube sections, side by side, but upper and lower sections were different. This means that the surface roughness of as-received tubes does not have an important effect on observed deposition as might be expected for these conditions which were deposition with significant entrainment.

This joint effect has been observed many times, but not always. The joint effect can be quite pronounced (as shown in Figure 9) for which two deposition lengths were simultaneously run in parallel. The comparison is between a 12 ft tube length alongside two joined 6 ft tube lengths. For the continuous 12 ft length, the deposition profile is linear over a large fraction of the length. In comparison, combined joint effects and end effects are shown for the two joined 6 ft tubes. Although the deposition profiles are quite different, the percent deposition over the total length was within 3% in both 12 ft tubes (18% in one and 12% in the other). This is well within the other uncertainties in predicting deposition.

REPRODUCIBILITY

As in other experimental work, the accuracy, reproducibility, and consistency of the deposition experiments were dictated by the control exercised over the independent variables entering into the final assessment of deposition velocity. Variables of flow rate, tube diameter, and particle size were recognized as being the most important variables to control. Careful calibration of the flowmeters used in these studies permitted average

NOMENCLATURE

A = cross sectional area of tube, cm^2

C = average particle concentration per unit tube volume downstream in the tube, particles/cm^3

C_o = average particle concentration per unit tube volume upstream in the tube, particles/cm^3

d = particle diameter, assuming spherical shape, cm

D = tube inside diameter, cm

$\mathcal{D}$ = diffusivity, cm^2/sec

f = Fanning friction factor, dimensionless

G = mass generation rate within containing system, particles/(cm^3sec)

$\bar{J}^{(1)}$ = mass flux due to concentration gradients, particles/(cm^2sec)

$\bar{J}^{(t)}$ = mass flux due to turbulent diffusion, particles/(cm^2sec)

K = deposition velocity, cm/sec [number of particles depositing/(cm^2sec)/ average number concentration/cm^3 of air]

L = distance from upstream to downstream points of interest in tube, cm

m = mass of individual particle, g

$\vec{n}$ = unit normal to the flow surfaces, dimensionless

N = mass flux, particles/(cm^2sec) or total flux at r, particles/sec

p = gas pressure, g mass/(cm sec^2)

r = radial distance measured from tube centerline, cm

R = Radius of tube, cm

Re = Reynolds number, $DV\rho/\mu$

S = surface containing continuity system, cm^2, and also stopping distance, $\frac{mv_o}{3\pi\mu d}$, cm

S^+ = reduced stopping distance, $\frac{SV\rho}{\mu}\sqrt{f/2}$, dimensionless

The deposition velocity data may be applied in macroscopic models [10, 13, 14, 15, 54, 55, 56, 57, 58] which are the integrated forms of the continuity equation. These models are usually written in general terms and include as variables, the deposition velocity, diffusivity, and re-entrainment constants, as well as radioactive decay constants. However, all of the constants have not as yet been fully evaluated. Models are still needed to fully describe deposition. Once deposition can be more successfully predicted from theoretical models, these models may then lead to a better understanding of deposition on surfaces with more complex geometry such as vegetation. [59, 60, 61, 62]

One important application of these deposition data is that of evaluating particle sampling errors when sample delivery lines must be used. From the data presented, reasonable estimates can be made of the degree to which a sample may be distorted by deposition in a line. Extrapolation and interpolation will be required to evaluate the deposition losses for conditions other than those reported here. As important as deposition errors may be, other sources of error must also be taken into account. These include errors from anisokinetic sampling, [48, 53, 63, 64] errors in using diverging collection nozzles, [64] losses in tube elbows, [49, 57, 65, 66] Brownian diffusion, [67] gravity settling, [52] electrical effects, [68] and agglomeration effects. [69]

ACKNOWLEDGEMENTS

I gratefully acknowledge the valuable suggestions and comments of Lysle C. Schwendiman, the computer solution of the diffusion equations by Clarence A. Oster, and the experimental assistance of M. Keith Thomas.

CONCLUSIONS

We have started from a continuity equation for particles to determine the assumptions that have been made in models to predict deposition. The principal assumptions are: 1) that the eddy diffusivity of particles is equal to the eddy diffusivity of the air, and 2) that particle deposition occurs by diffusion up to a free-flight distance from the wall. The assumption of a particular velocity to calculate the free-flight distance is a useful modeling concept. However, the particular velocity used is questionable since the particle velocity has been assumed to be equal to either the radial rms air velocity at a distance y^+ of about 80 or the radial rms air velocity at the start of the free-flight distance. The true velocity is probably between these two limits. Nevertheless, free-flight distances are used in the more successful models which are those of Friedlander and Johnstone and this author. The velocities at the start of the free-flight are in serious disagreement for these two models. Nevertheless, both models appear to predict a range of deposition velocities which tend to agree with the experimental data. Modeling concepts must be improved to obtain closer agreement with the experimental data.

This author is continuing work on this subject and will also search for a model which will describe deposition when an inverse profile exists.

Since theories do not fully predict deposition, and therefore, do not predict adequate correlation parameters, the present data have not been presented in a general form. The data show, however, that graphical representation of the data plotted as K/V versus S^+ is not an adequate correlation.

The principal effects of particle size and tube Reynolds numbers on deposition have been shown for the range of variables studied. In most cases, the deposition can be represented by deposition velocities. However, other cases are not adequately represented, and indeed, are not adequately understood. These cases are for re-entrainment conditions, end effects, internal effects, and joint effects. All these secondary variables affecting deposition are now of increased importance as the primary effects on deposition velocities of particle size, Reynolds number, and tube size have been shown.

the 0.21 in. ID tube, that the smoothed experimental curve is a good representation of the deposition data for 2 μ diam particles. These data were selected for comparison since the data extend over nearly the maximum range of experimental deposition velocities, and also since inverse profiles probably do not exist for these conditions. The absence of inverse profiles is important since the diffusional mechanisms used in all the models could not allow the existence of the inverse profiles. Further modeling improvement is planned to include the case of inverse profiles.

From Figure 15, one can see that the theories of Friedlander and Johnstone and this author predict the same general trend and are in fair agreement with experiment for deposition velocities above 1 cm/sec. Equation (53) is essentially the same as Davies' theory, except that this author uses cylindrical coordinates in the derivation. Davies' assumption that turbulent diffusion of particles to a circular tube wall could be treated as diffusion from the flowing gas to a plane surface is too great a simplification for the operating conditions shown. The model by Owen predicts a curve which crosses the experimental data, but we must remember that Owen's curve is independent of particle size. To calculate Owen's curve, we assumed that the concentration was 1 particle/cm^3. For different concentrations, the predicted deposition velocities would be directly proportional to particle concentration.

The theories of Friedlander and Johnstone and of this author appear to show the best agreement between theory and experiment as well as between theories. The agreement between theories is surprising because of the assumptions in the models. In the models of Friedlander and Johnstone, particles are assumed to have a radial velocity of $0.9u_*$ which is an air velocity far from the surface. The particles diffuse from a y^+ distance of 30 to the distance S^+ at which time free-flight to the wall occurs by the velocity $0.9u_*$. In comparison, the velocity for free-flight in the author's model is assumed to be imparted to the particle only at the distance S^+, and the velocity is characteristic of the root mean square air velocity at distances both far and near to the tube wall. This discrepancy as well as discrepancies between theory and experiment must be resolved. Further modeling is planned.

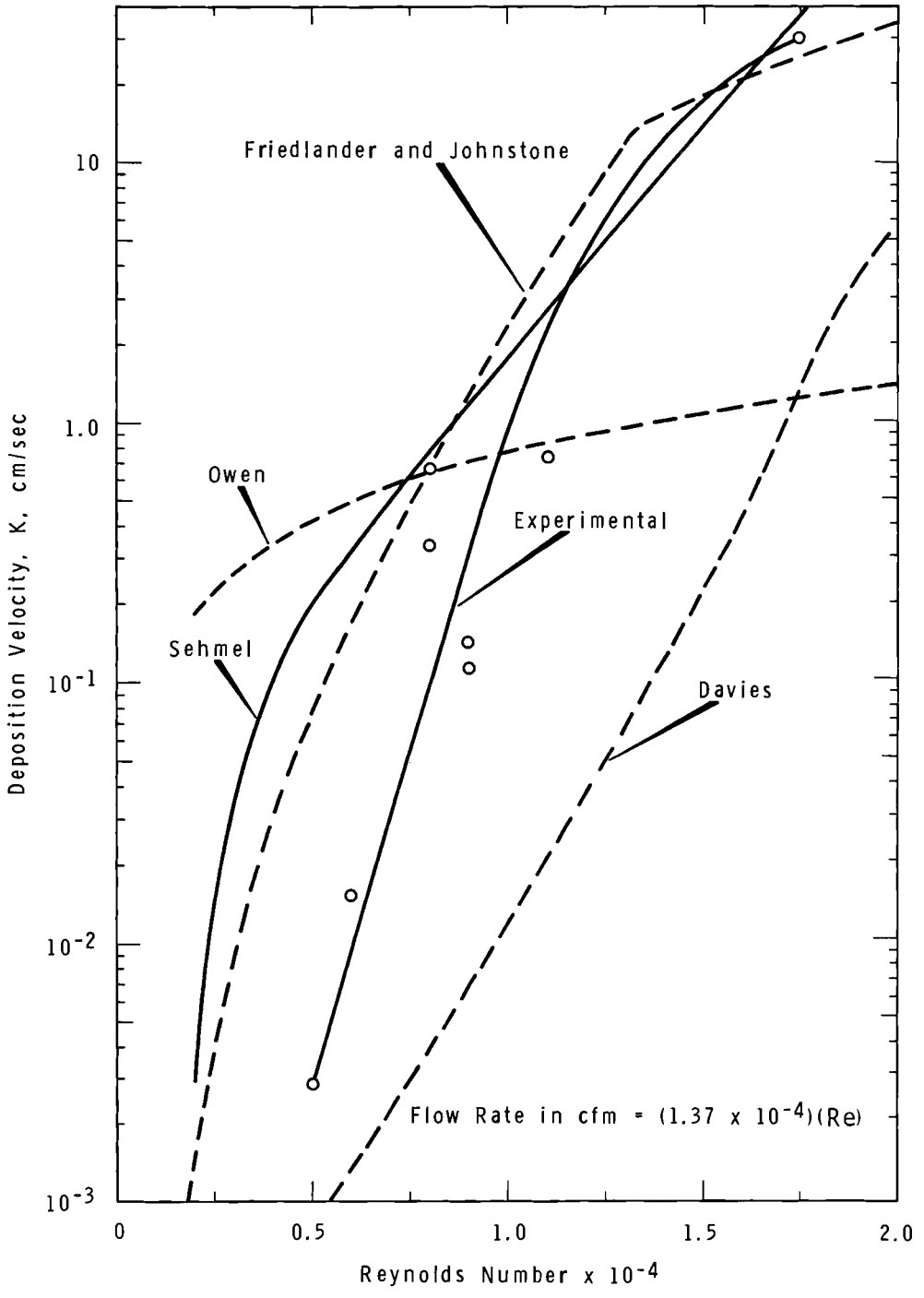

Neg 0672863-4

FIGURE 15. Comparisons of Theoretical Predictions and the Experimental Deposition Velocities for 2 μ Diam Particles in 0.21 in. ID Tubes

However, the possibility of vortex flow[50] was eliminated. Liquid uranine was inserted through a small hole in the 2.81 in. ID tube wall while the air flow was turbulent. Examination of the tube showed no vortex action on the uranine trace along the wall.

For the operating conditions of Figure 14, the deposition would still be increasing if the flow rate were increased. This increased deposition means that the inverse profile may be caused by re-entrainment, but re-entrainment as measured by total deposition at a S^+ value of about 10 has not occurred. Thus, the inverse profile is a condition of high particle deposition, and the inverse profile does not fit into the diffusive flux models of Equations (48) and (53). If the velocity profiles were factored into the inverse loading profiles, the resulting inverse concentration profile would be even more pronounced.

The inverse profile is seen to disappear for 12 μ particles, if the tube is covered with petroleum jelly which acts as a tacky surface. This inverse loading profile is obtainable downstream of the tacky surface, if as-received tubing is used. The transient back to the inverse profile was shown to occur within a 10 ft length of tube. However, the transient probably occurs in a shorter tube length.

The data for 6 μ particles show that the loading profiles are relatively unaffected by the pressure drop across the filter. The pressure drop across a high efficiency glass fiber filter was 78 in. H_2O. This was the standard filter type used for particle collection. In comparison, the pressure drop across a very open structured filter was only 3 in. H_2O. As seen in Figure 14, the measured concentration profiles were the same for each filter type.

COMPARISON WITH THEORETICAL PREDICTIONS

The theories of Friedlander and Johnstone, Owen, Davies and the author were used to predict the theoretical deposition curves shown in Figure 15. These four curves are to be compared to the experimental data which are represented by the same smoothed curve previously shown in Figure 2. We can see from Figure 2 that in relation to all the data for

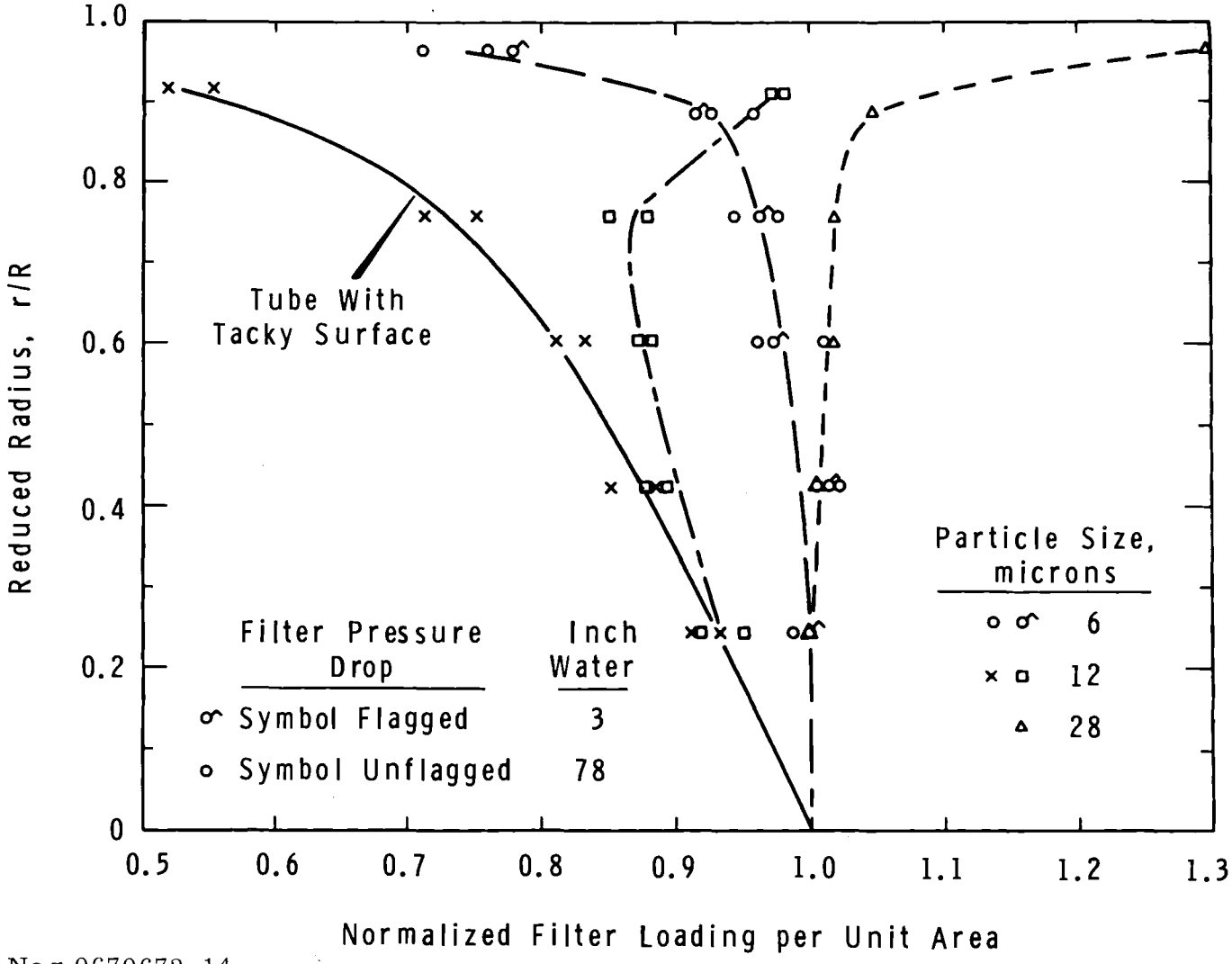

Neg 0670672-14

FIGURE 14. Particle Filter Loading Profiles at a Reynolds Number of 55,000 (98 cfm) in a 2.8 in. ID Vertical Tube

near the wall is greater for the tacky-surfaced tube than for the as-received tube. Since we assume the diffusion coefficients are equal, the concentration gradients are directly proportional to the diffusive fluxes. Thus, we would predict from the filter loading that the deposition of 2 μ particles is greater for the tacky-surfaced tube. Deposition measurements confirm this prediction. The comparison is made for deposition using the data for an untreated 118 in. long tube which was immediately upstream of the 24 in. long tube which had the tacky surface. The deposition for the untreated tube was 0.139 to 0.169%, and for the tacky tube 0.178 to 0.229%. This means that about 30% more particles deposited in a 24 in. section of tacky tube than in a 118 in. section of untreated tube, or that the effective deposition flux is over six times [(1.3)(118/24) = 6] greater in the tacky tube. We conclude for these operating conditions that radial concentration profiles do exist, and for a constant particle size deposition increase as the concentration gradient increases. A necessary conclusion in explaining the two different concentration gradients is that the boundary conditions are different; that is, if we neglect any air drag difference due to the tacky surface, a difference must exist in the particle accommodation coefficient for each surface. Since the deposition would be increased by an increase in air velocity, these operating conditions are not those characterized by re-entrainment by decreased deposition velocities for S^+ values greater than about 10. Stated differently, we conclude that even for this low deposition, 2 μ particles may be re-entrained unless the accommodation coefficient is increased toward unity by making the surface tacky.

The single concept of deposition by a diffusive flux of Equations (48) and (53) appears to be most valid, if the accommodation coefficient is near unity. The complexities will be illustrated by the filter loading profiles shown for three particle sizes in Figure 14. The three facts to be noted are that the filter-loading profiles are a function of particle size, may exhibit a maximum in the annulus adjacent to the tube wall, and are relatively unaffected by the pressure drop across the filter. For simplicity of discussion, an increase in the filter loading as the wall is approached will be termed an inverse loading profile. The mechanisms[7] for causing the observed inverse profiles have not yet been determined.

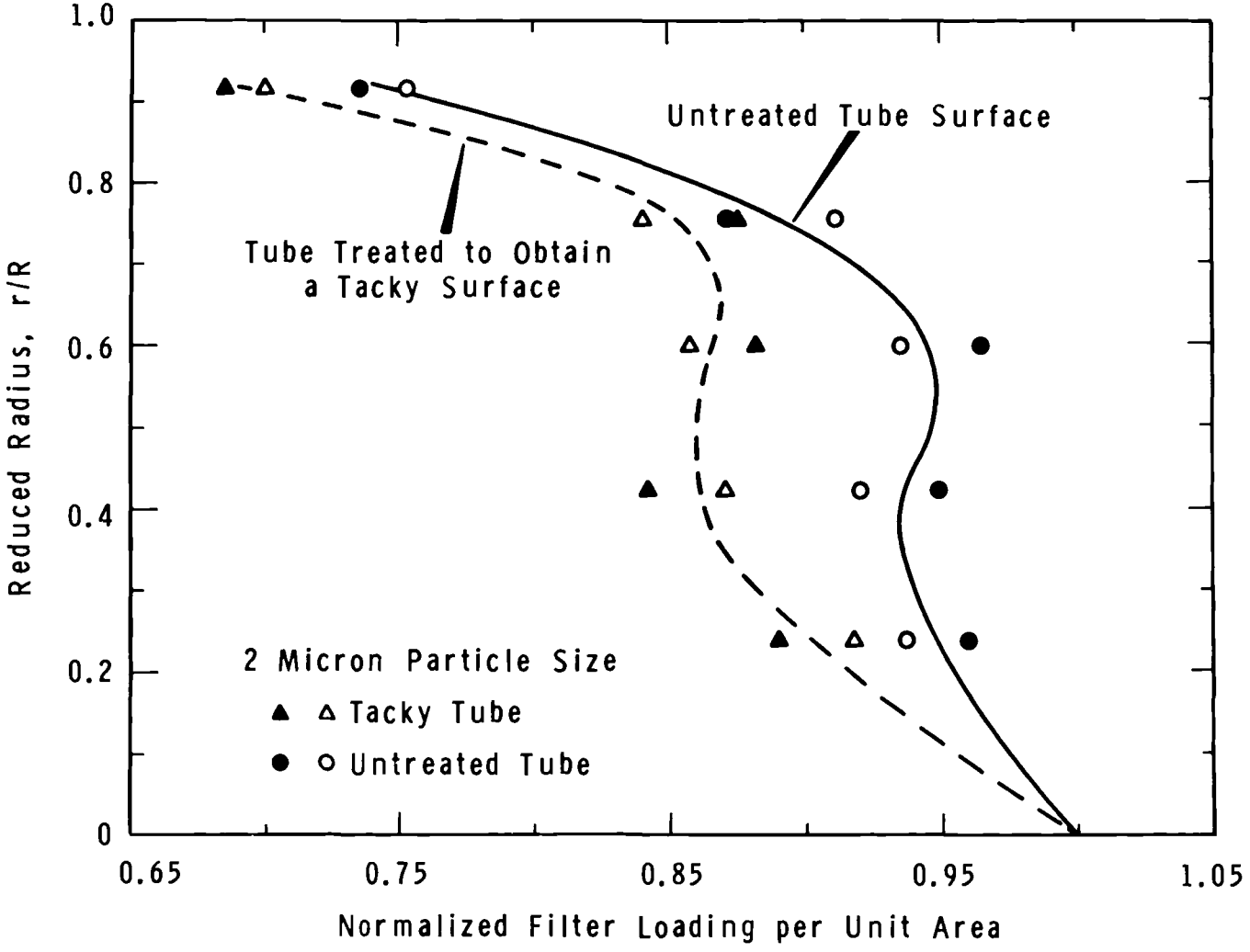

Neg 0670672-10

FIGURE 13. Effect of Tube Surface on Particle Filter Loading Profiles Within a 2.81 in. ID Tube at a Reynolds Number of 36,000 (64 cfm)

collected on the filter may be moved radially due to the velocity flattening. However, this flattening[52] is considered to be minimal, since both low and high pressure drop filters indicate the same collection profiles on each filter as will be shown.

The filter was cut into annular sections with dimensions as were given in Table I, the sections analyzed fluorimetrically for the uranine particles, and the filter loadings on each annular section then normalized to the filter loading per unit which are on the filter center section of 0.4 in. diam. These normalized filter loadings are plotted in Figure 13 at the mid-point of each filter annular section. Curves are compared for a tube with an inner surface made tacky with a thin layer of petroleum jelly, and for an untreated tube surface. As expected, these filter loading profiles show a general decrease in loading as a function of radius. This decrease in loading was expected since the deposition of 2 μ particles is very low—these particles tend to follow the average motion of the turbulent air. These loading profiles were integrated to obtain the ratio of the average loading across the filter central section. These ratios are compared in Table II to the ratio of the average velocity in the tube.

TABLE II. Average Profile Comparison

	$\frac{\text{Average Loading}}{\text{Central Loading}}$	$\frac{\text{Average Velocity}}{\text{Maximum Velocity}}$
Tacky Tube	0.814 - 0.809	0.82
Untreated Tube	0.868 - 0.869	0.82

This table shows a reasonable agreement between filter loadings and velocity profiles. However, the double curvature in the loading profiles was unexpected and may be due to experimental error.

The particle filter loadings next to the wall are of prime interest in our consideration of deposition mechanisms. We have assumed that the deposition flux is as given by Equation (48), and is equal to the product of a turbulent diffusion coefficient and a concentration gradient. We assume that the turbulent diffusion coefficient is relatively unaffected at a distance from the wall by changing the tube surface from as-received to tacky. Now we see from an inspection of Figure 13 that the concentration gradient

to 15 μ diam and larger particles, if the tube wall is dry. This development yields a criterion for re-entrainment that y_d^+ be greater than about 0.4.

RADIAL CONCENTRATION PROFILES

The axial flux of particles as a function of tube radius was determined for turbulent flow within a vertical tube. The ratio of the flux of particles per unit cross sectional area divided by the local velocity is the particle concentration as a function of tube radius. The particle concentration is important in determining the mechanisms of particle deposition on the tube wall. However, this concentration has not been directly measured in the present study, since the velocity profiles were not measured. The particle flux profile would be equal to the concentration profile, if the air velocity were independent of radial position. Actually, the velocity profile is such that the ratio of the maximum to the average velocity increases from 0.5 for laminar flow to about 0.8 to 0.9[9] for turbulent flow. However, the effects of velocity profiles are neglected at this time in determining the particle concentration profiles. The following work will show that radial concentrations exist throughout a tube in turbulent flow.

The first indication that concentration profiles existed within a tube was from a series of isokinetic samples[48, 49] taken from the center line of a 2.81 in. ID tube. The sampling velocity was set to correspond to the center-line flow in the tube. For uniform concentration in the radial direction, the concentration from the isokinetic sample should be equal to the concentration obtainable from the ratio of all particles passing through the tube, divided by the total flow through the tube. However, the sample concentration and the average tube concentration were not the same. For constant sampling conditions, the relative concentration of particles collected in the isokinetic sample decreased from that of the tube average as the particle size increased from 1 to 28 μ.

The conclusion obtained from these isokinetic samples is that, in turbulent flow, the particles are nonuniformly distributed across a tube[26, 50, 51]. This nonuniformity was determined as a function of the tube radius by placing a filter completely across the tube center. The filter will tend to flatten the velocity profile; and hence, the particles

The laminar sublayer depth is generally conceded to be that distance from the tube wall which makes the dimensionless parameter, y^+, equal to 5, with y^+ defined by

$$y^+ = \frac{y V \rho \sqrt{f/2}}{\mu} \tag{61}$$

in which y is the distance from the wall to the point being considered in the fluid.

A distance from the wall equal to the particle diameter, d, may be specified and expressed in terms of y^+; then,

$$d = \frac{y_d^+ \mu}{V \rho \sqrt{f/2}} . \tag{62}$$

This relationship is merely a statement that the dimensionless y_d^+ has been calculated at a position away from the wall equal to d. If d in this relation is substituted in Equation (59) for the reduced stopping distance, S^+, then an expression for y_d^+ as a function of S^+ follows:

$$y_d^+ = \left[\frac{20 \rho S^+}{\rho_p}\right]^{1/2} . \tag{63}$$

This equation permits the calculation of y_d^+ corresponding to a distance from the wall equal to d in terms of stated S^+. This relation is plotted at the bottom of Figure 12 for 2.81 in. ID tubing. For these conditions re-entrainment occurs between S^+ values of 2 to 6 for the untreated tubes. Similarly, for the smaller tube sizes, re-entrainment occurs at S^+ values of about 10. Substitution of S^+ of 10, ρ_p = 1.5 gm/cm^3, and $\rho = 1.2 \times 10^{-3}$ gm/cm^3 into Equation (63) yields $y_d^+ \simeq 0.4$. The significance of this result is that a y^+ of 0.4 represents a point about 0.08 the distance from the wall to the boundary of the laminar layer ($y^+ = 5$). Unless turbulent eddies penetrate to within about one particle diameter of the tube wall, it is unlikely that the particles will be re-entrained. A necessary conclusion is that the laminar sublayer must be frequently and deeply penetrated by eddies with sufficient energy to re-entrain 10

modified Reynolds number,

$$\frac{d\ V\ \sqrt{\rho\rho_p}}{\mu} \quad . \tag{60}$$

This correlation appears to be about as good as plotting the deposition ratio versus the reduced stopping distance, or a modified form of the reduced stopping distance, which required use of dimensional constants.[21] These correlating parameters mask the deposition behavior as determined by using single-sized particles from the spinning disc aerosol generator. An adequate single parameter is yet to be established. In a later section of this report some comparisons will be shown between deposition predicted by several models. These comparisons show the generally unsatisfactory agreement among models and with experiment, and give indications why a single parameter based on these models will likely fail to correlate the data.

Some observations made during the course of this work have led to insight into the even more complex nature of particle motion in turbulent flow than heretofore assumed, and these observations help explain why existing models fail to predict deposition adequately. Further elucidation of particle retention and re-entrainment was also obtained and will be discussed briefly.

BOUNDARY LAYER CONCEPTS

Features of the boundary layer can be deduced from the deposition data. For the basis of the discussion we will consider that particles approach the wall and deposit. Subsequently, the particles either remain or are re-entrained. The conditions for re-entrainment[37, 38, 41, 42] can furnish better understanding of the boundary layer.[43, 44, 45, 46, 47]

We sought a parameter to determine the onset of re-entrainment. A parameter was indicated when the deposition ratios, K/V, were plotted versus the reduced stopping distance, S^+. From this plot we concluded that re-entrainment occurs for S^+ values greater than about 10, and that at the onset of re-entrainment, turbulent eddies must be penetrating[39] deeply into the classic laminar sublayer. The following considerations lead to this conclusion.

$$S^+ = \frac{d^2 \rho_p V^2 \rho f}{40 \mu^2} \quad (59)$$

in which d = particle diameter
f = Fanning friction factor
V = average air velocity
μ = air viscosity
ρ_p = particle density
ρ = air density.

For the untreated tube, effective re-entrainment is occurring between S^+ values of about 2 to 6. For smaller size tubes, re-entrainment[39] occurred at an S^+ of about 10. For the tacky-surfaced tube, re-entrainment has not occurred for S^+ values as high as 40.

CORRELATION PARAMETERS

Deposition velocity data have been presented as a function of Reynolds numbers and particle sizes for vertical aluminum tubes with inside diameters of 0.21, 0.62, 1.152, and 2.81 in. Although useful in this form, the data would be more easily extrapolated and interpolated to other than the experimental conditions, if an overall correlating parameter could be found.

The author[21] has used a dimensionless plot of the deposition ratio, K/V, versus the reduced stop distance, S^+, to correlate the data from polydispersed particles of Friedlander and Johnstone[1] and of Postma and Schwendiman.[31] This use of the reduced stop distance as the independent variable was based upon the form of Friedlander and Johnstone's equation to predict the deposition ratio. A rather general correlation was obtained. The reason for the scatter of the data around the correlation curve becomes apparent when the smoothed curve of Figures 2 through 5 are plotted on similar coordinates of K/V versus S^+. These smoothed curves would show multiple curves crossing through the correlation curve.

Polydispersed particle data have also been correlated by Epstein and Evans[40] who have plotted the deposition ratio, K/V, versus a

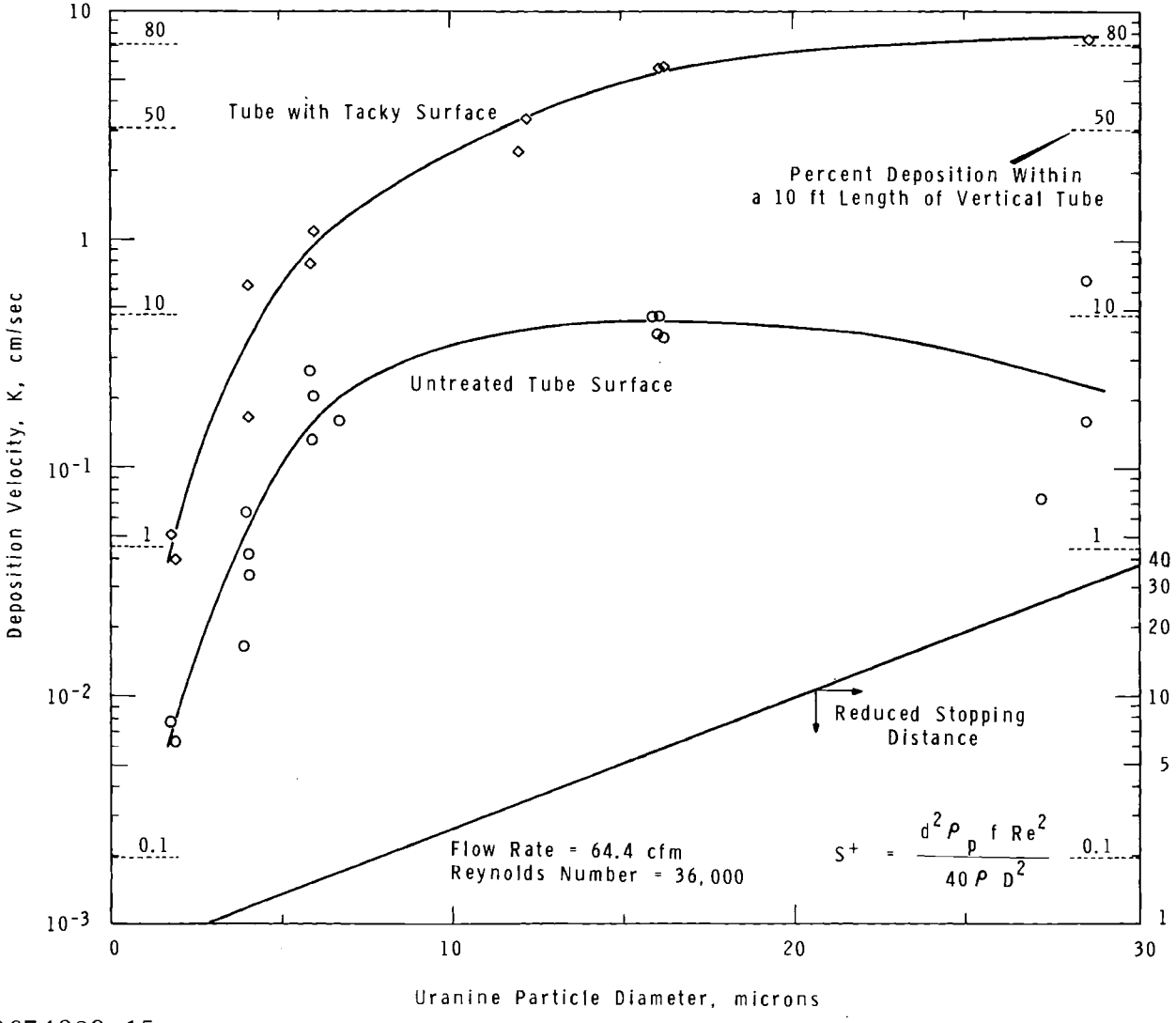

Neg 0674029-15

FIGURE 12. Effect of Tube Surface Treatment on Deposition in a 2.81 in. ID Vertical Tube

The deposition velocity is relatively independent of particle size for diameters larger than about 8 μ for a Reynolds number of 4200. Deposition velocities increase rapidly with particle size for a Reynolds number of 21,000. For the two higher Reynolds numbers, the deposition velocities increase with particle size until a particle size is reached at which marked re-entrainment is indicated by the rather abrupt decrease in the deposition velocity. For particles larger than about 8 μ and high Reynolds numbers of 3.6×10^4 and 5.5×10^4, the effective deposition velocities decrease or remain essentially constant as the particle size is increased.

Re-entrainment at a particle size of 8 to 16 μ can be prevented by coating the internal surfaces of the tube with petroleum jelly which serves as a near perfect sink for particles. Comparison of deposition velocities for a tacky-surfaced tube and an untreated tube are shown in Figure 12 for the 2.81 in. ID tubing. The deposition velocities for the tacky-surfaced tube are much higher than for the untreated tube. For particle sizes greater than about 15 μ, the deposition velocities increase more slowly with an increase in particle size.

The deposition data for 2 μ particles suggest that all of the 2 μ particles striking an untreated surface do not remain on the surface, since deposition on the tacky surface is significantly greater than for the untreated tube surface. These are the first deposition data showing that for particles as small as 2 μ some rebounding or re-entrainment may occur for an untreated tube. An "accommodation coefficient" appears to be required to account for these observations.

The short broken lines on either side of Figure 12 show the percent deposition within a 10 ft length of vertical tubing. The maximum shown is about 10% for 16 μ diam particles in the untreated tube. In comparison, the deposition is also about 10% for 5 μ diam particles in a tacky surface tube. For 28 μ diam particles, the deposition is over 80% in a 10 ft length of tacky surfaced tube.

Shown in the lower right corner of Figure 12 is a relationship between particle size and the reduced stopping distance,

The dry wall does show re-entrainment as indicated by the lower branch of the 8 to 9 μ diam curve. The lower curve branches again at a Reynolds number of 4.5×10^4. This second branching is an indication that a combination of tube surface properties and particle properties are important in determining the total deposition for re-entrainment conditions. For this second branch, the particles in the upper branch were not as dry as determined by microscope examination of cascade impactor samples as they appeared to be for the lower branch.

The data symbols for Reynolds numbers less than about 10^4 and deposition velocities less than about 10^{-3} cm/sec are not represented by solid curves. For this region we have two problems. The first is that deposition is low and hence these data were determined from washing 12 ft lengths of tubing. Since the deposition was low, end effect deposition may be relatively more important in the overall deposition. The second problem is that we may be approaching the minimum deposition velocity between that due principally to Brownian motion and that due principally to turbulent motion. Figure 4 shows a possible indication of this minimum. For a Reynolds number of about 2000, the deposition velocity of 1 μ particles is shown to be about 10^{-3} which is greater than the deposition velocity of 10^{-4} for the 6 to 9 μ particles. Considering only turbulent deposition mechanisms, the deposition velocity of 6 to 9 μ particles should be greater than that for 1 μ particles. Thus, we conclude that these data for 1 μ particles may be in the minimum region, but additional data are needed to resolve the question.

The deposition velocities for the largest tube size studied of 2.81 in. ID are shown in Figure 5. Tube surfaces were as-received for this tube size. The deposition velocities are shown as a function of particle size with Reynolds number as a parameter. The particle size range is extended above 8 μ to a particle diameter of 29 μ. The larger particles above about 20 μ were wet spherical particles, as compared to dry spherical particles for particles below about 10 μ. An important observation is that the maximum measured deposition velocity is only of the order of 1 to 2 cm/sec as compared to the 10 to 30 cm/sec for the smaller tube sizes. This difference in the maxima will lead to difficulties in representing the deposition data for all tubes by a correlation.

curve. Above 10^{-3} cm/sec the curves are well defined. These data do not show the effect of particle re-entrainment as will be shown for the large diameter tubes.

In Figure 3 the deposition velocities are shown for the same particle size range for a larger tube size of 0.62 in. ID. For deposition velocities greater than about 10^{-3} cm/sec, the deposition velocities for each particle size increases rapidly with an increase in Reynolds number until a deposition velocity of about 10 to 30 cm/sec is reached. For additional Reynolds number increases, the deposition velocities increase slowly or tend to remain constant. A decrease would identify the onset of effective particle re-entrainment. The valley in the solid curve at a Reynolds number of 1.5×10^4 for the 8 μ diam particles and the concave downward trend for 4 to 6 μ particles show a consistent trend, but the cause for the valley is unknown.

In Figure 4 the deposition velocities are again shown for the same particle size range, but now for a larger tube inside diameter of 1.152 in. Similarly, in Figure 3, the data symbols are represented by smoothed solid curves and the calculated percent depositions within a 10 ft length of tubing are represented by the broken line curves. A further similarity is that a valley occurs for the 8 to 9 μ particles at a Reynolds number of 2×10^4. For higher Reynolds numbers the similarity ends for these 8 to 9 μ particles. The curve is split into two branches at a Reynolds number of 2×10^4. The upper branch is for a tacky coated tube and the lower branch is for particle re-entrainment conditions for as-received tubes.

The tacky-coated tube was an as-received tube coated with a thin layer of petroleum jelly. This coating was to simulate the case of a perfect particle sink at the tube wall. The data for the tacky coated tube are indicated by flagged symbols. These flagged symbols are in the upper branch of the curve as well as along the curve before it branches. The flagged and unflagged symbols between Reynolds numbers of 1×10^4 to 1.5×10^4 show an overlapping scatter. This means that for these deposition conditions both a dry wall and a tacky-coated wall act as similar perfect sinks.

The reproducibility for essentially replicate experiments can be exemplified by the data for experiments using 8 μ particles at a Reynolds number of 1.1×10^4 shown in Figure 4. For these 12 data points (including two for internally coated tubes to make them tacky), the deposition velocities range from about 2.8×10^{-3} to 2.5×10^{-2} cm/sec which correspond to a total deposition of from 0.25 to 0.65% in a 10 ft length of tubing. The causes for this range of depositions are not readily identified, but the range is somewhat surprising in light of the excellent reproducibility and consistency achieved for data plotted in Figures 8, 10, and 11.

Exacting control of the variables of particle size, density, and quality are important in achieving reproducibility, as are also the precision in measurement of velocity and tube dimensions. Figures 7 and 9 present data for experiments in which particles were drawn simultaneously from the same aerosol chamber with negligible velocity differences. The rather large differences in deposition suggest that one or more variables, yet to be identified, may be effective under some conditions. Notwithstanding the variability among individual data points, the data taken as a whole show the importance of critical parameters and permit a good measure of particle retention under many conditions.

DEPOSITION VELOCITIES

Deposition velocities were determined for tube sizes of 0.21, 0.62, 1.152, and 2.81 in. ID. In Figure 2, the deposition data are shown for 0.21 in. ID tubing as a function of Reynolds number for particles of several sizes. The data symbols are represented by the smoothed solid curves and illustrate that deposition increases rapidly as the flow rate is increased. The solid curves are for 8, 4-5, 2, and 1 μ diam particles. These solid curves are intercepted by broken line curves which show the calculated percent deposition within a 10 ft length of vertical tubing. For instance, at a Reynolds number of 3300 (flow rate in cfm = $1.37 \times 10^{-4} \times 0.33 \times 10^4 = 0.45$), the deposition would be 99% of 8 μdiam particles. In contrast for the same flow rate, less than 1% of 1 μ diam particles would be deposited within the same 10 ft length of vertical tubing.

The deposition velocities are from about 10^{-4} to 30 cm/sec. Below 10^{-3} cm/sec, the data show too much scatter to sufficiently define a solid

In an almost identical experiment (results shown in Figure 8), reproducibility was excellent. Differentiating surface quality by visual observation was not possible as judged by the nearly identical deposition profiles for the tubes. Again, re-entrainment conditions prevailed.

Results already described and presented in Figure 9 show another example of relatively poor reproducibility (though considerably better than that shown in Figure 7), presumably due to a joint in one tube. End and joint effects may introduce additional uncertainties in deposition measurements.

For the non-re-entrainment conditions maintained for the experiments whose data are shown in Figure 11, one might entertain the conclusion that as-received tube surface variations are not as important in their effect on net deposition in non-re-entrainment cases as for the entrainment conditions. For example, see Figure 7. One might logically expect that particles once deposited on a relatively rough surface may be retained to a significant degree due to protection from re-entrainment by surface features of fine cracks, ridges, etc. Because surface irregularities could be quite variable, the degree to which the net deposition is affected (for re-entrainment conditions) might be significant. Greater variation in measured net deposition would be anticipated, if the net deposition was the end result of initial deposition and subsequent re-entrainment or re-bounding. Although born out by the data in Figure 7 which are for identical parallel runs with different as-received tubes, the conclusion is not supported by the data obtained and shown in Figure 8 in which excellent reproducibility was obtained for two tubes selected at random. In Figure 9, which presents data for an experiment for conditions identical to those maintained for Figure 7, somewhat better, but still rather poor reproducibility is shown than that in Figure 7. This experiment (see Figure 9) did involve the additional complexity of jointed tubes at the midpoint which had a marked effect on the resulting curve.

Although we have suggested a tentative, but qualitative, explanation for variability in cases where re-entrainment occurs, a review of Figures 2, 3, 4, and 5 will show that achieving good reproducibility has posed a problem for most operating conditions.

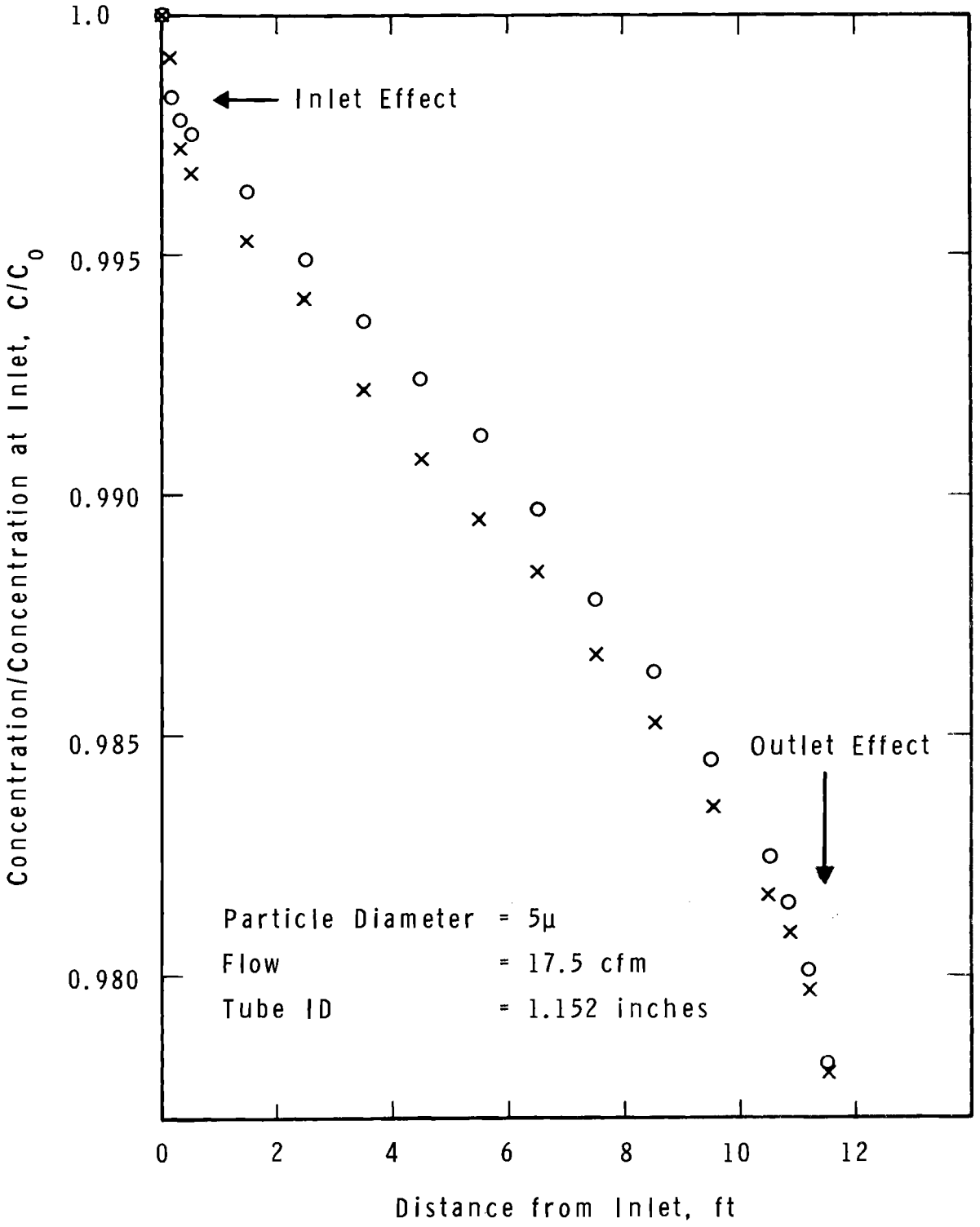

Neg 0672177-3

FIGURE 11. Aerosol Concentration Profiles Showing Reproducibility for Non-re-entrainment Conditions

boundary layer development. The reproducibility is demonstrated by the smoothness of the curve. There is an indication of small perturbation of the joints, but there is not a very significant break apparent in the slope. Not every profile was this consistently exponential as will be further discussed; however, a truly exponential profile shows that a narrow size range of particles is entering the tube, and allows a discrete, accurate evaluation of the deposition velocity.

Several experiments were performed in which nominally identical conditions were used. Particles were simultaneously drawn through parallel lengths of as-received tubes at identical rates, and the concentration determined as a function of distance along the tube. Figure 11 shows the results of one such experiment. Each concentration profile is for the center 12 ft of tubing which was joined, above and below, to identical sections. The two curves show the results from parallel sections. The end effects reproduce well, as does the overall concentration profile. Conditions of flow and particle size were selected for which re-entrainment was negligible.

Although tubes are nominally identical (within manufacturing tolerances), we have observed differences in identical runs which we can only ascribe to subtle differences in tube-surface quality. Two tubes were selected which appeared by visual observation to have a different surface quality. One tube was characterized as being "rough", by this examination. The tube showed somewhat more pronounced die markings than the second tube, classed as "smooth". The actual difference in surface quality was not highly discernible, and could not be further quantified with profilometers available. These two tubes were supported in parallel and 16 μ particles passed simultaneously through the tubes. Flow, particle size, and tube diameter were such that re-entrainment was significant. Figure 7, already briefly discussed, shows the concentration profiles inferred from the net deposition on the two tubes. Reproducibility must be judged to be poor in this experiment, and the observation is an anomaly which has not been resolved. The results certainly do suggest that some physical qualities of tube surface may yield unusual deposition.

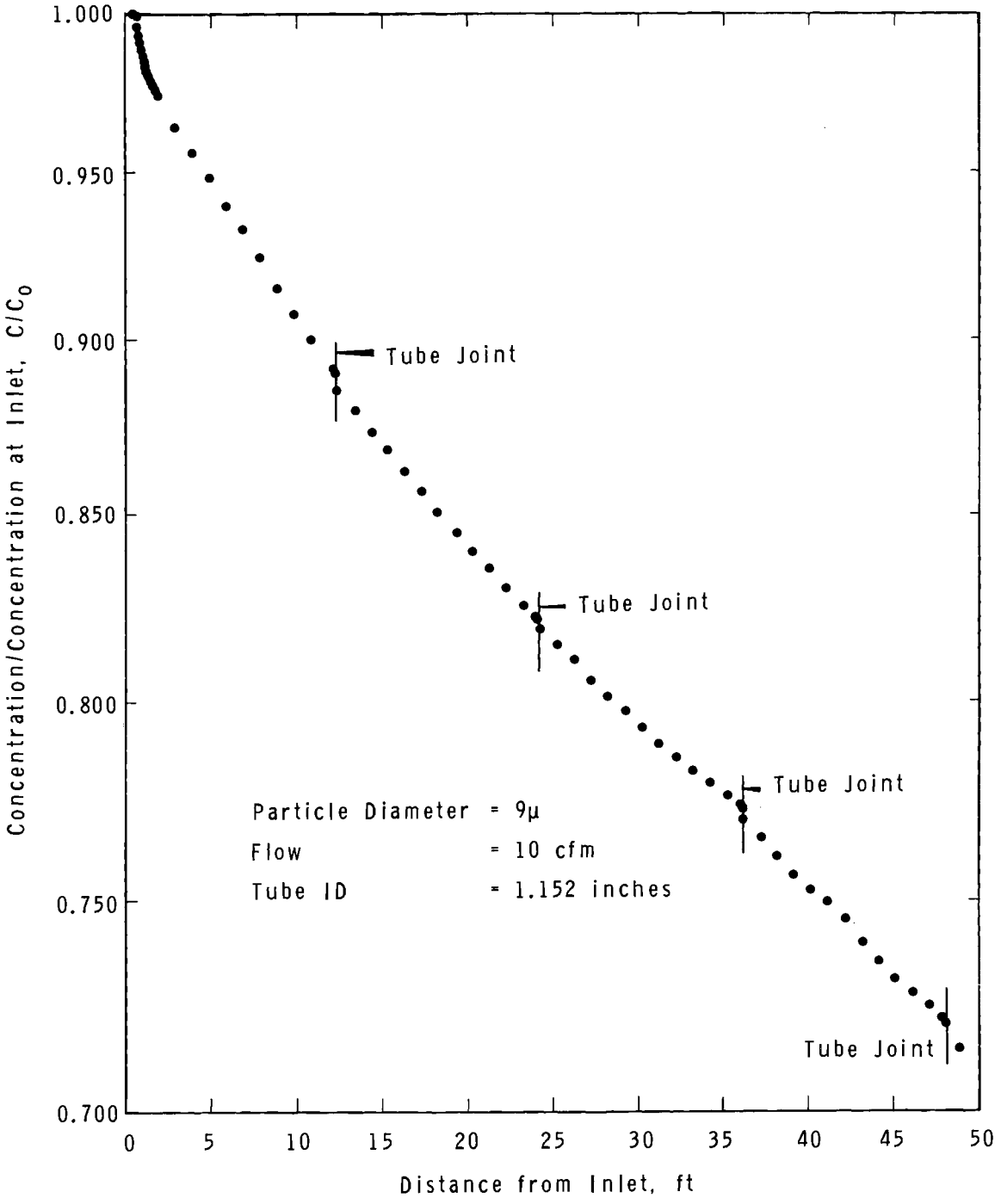

Neg 0672863-6

FIGURE 10. Aerosol Concentration Profiles Showing Deposition Velocity Reproducibility Along a 49 ft Length of Tubing

velocities to be measured within an estimated 2%. Particles were closely monodisperse and samples were taken frequently for sizing. Because the deposition velocity may increase with approximately the fourth power or greater of particle diameter, small errors in particle sizing may effect significant errors in deposition velocity. Tube diameters were held to manufacturer's tolerance and were not more than ± 0.002 in. from the nominal diameter. The evaluation of the mass loading of particles through fluorometric measurements can be shown to be a minor source of error. Measurements of fluorescence were all relative and stability checks of the instruments were made during every experiment. Manipulative errors are always present, but only simple operations were required, and this source is believed insignificant compared to other sources. Less easy to evaluate are errors arising from differences in the quality of the particle used, primarily the dryness of the particle. Larger particles dry more slowly and may be more sticky. Humidity changes could have an effect as well. These were not evaluated specifically. Other variables, such as joint effects already discussed, subtle differences in tube surface roughness, degree to which the longitudinal deposition profile followed the exponential relation, and vibration, may have introduced uncertainties in the finally evaluated deposition velocity.

Because many of the variables and their errors could not be evaluated discretely and objectively, we have used the reproducibility in essentially replicate runs as the primary index.

The following are some observations which help appraise the reproducibility of the data taken for these special experiments and the experiments as a whole.

The reproducibility of the manipulative and fluorimetric procedures can be inferred from Figure 10, in which the change in concentration is plotted from one experiment as a function of distance along the tube. Each point represents a short section of the tube and a separate analysis of uranine deposited. The total length of 49 ft consisted of four continuous 12 ft long sections and a 1 ft long section. The concentration profile shows some curvature, more pronounced at the inlet 4 ft which is attributed to

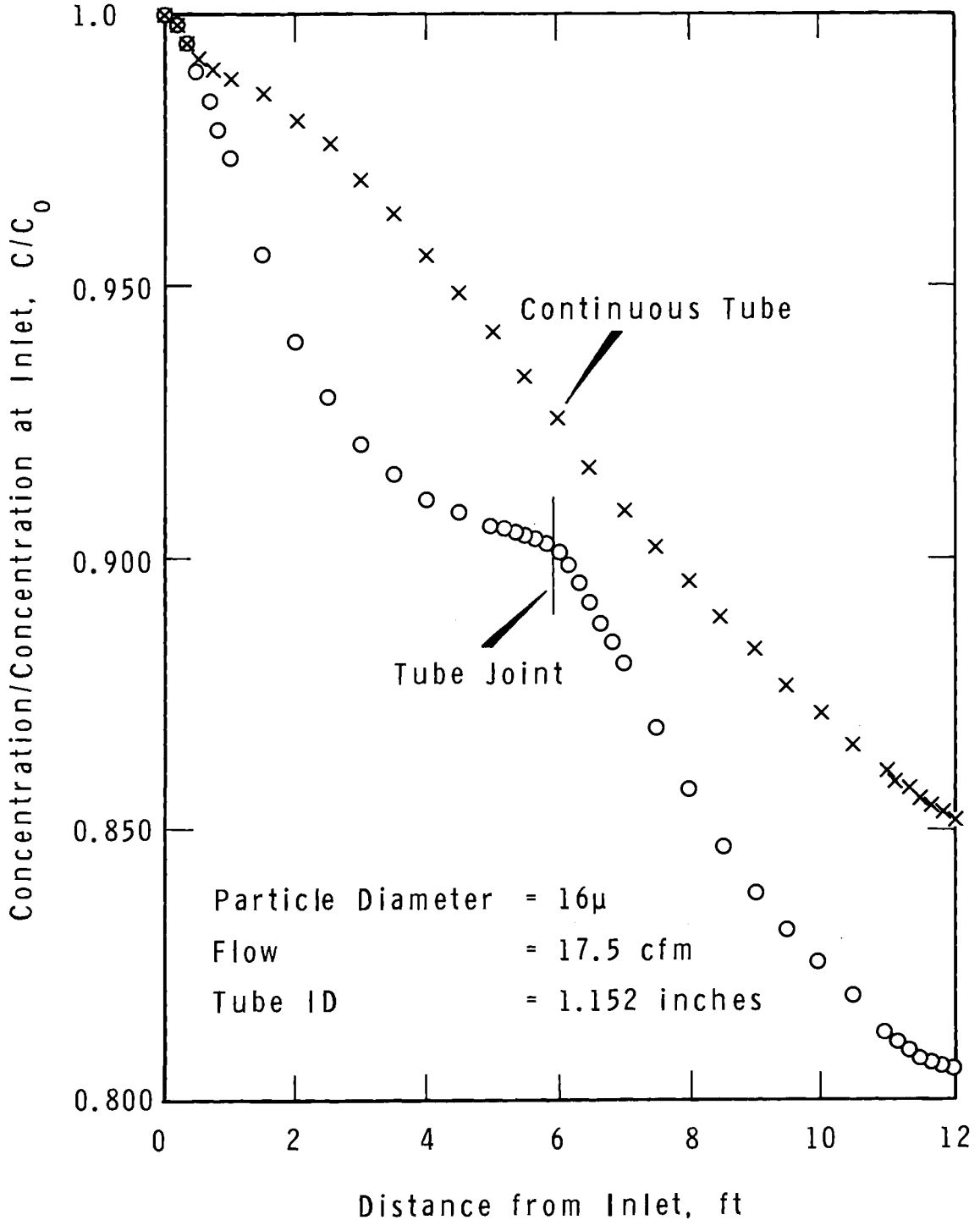

Neg 0672863-3

FIGURE 9. Aerosol Concentration Profiles Showing the Effect of a Tube Joint

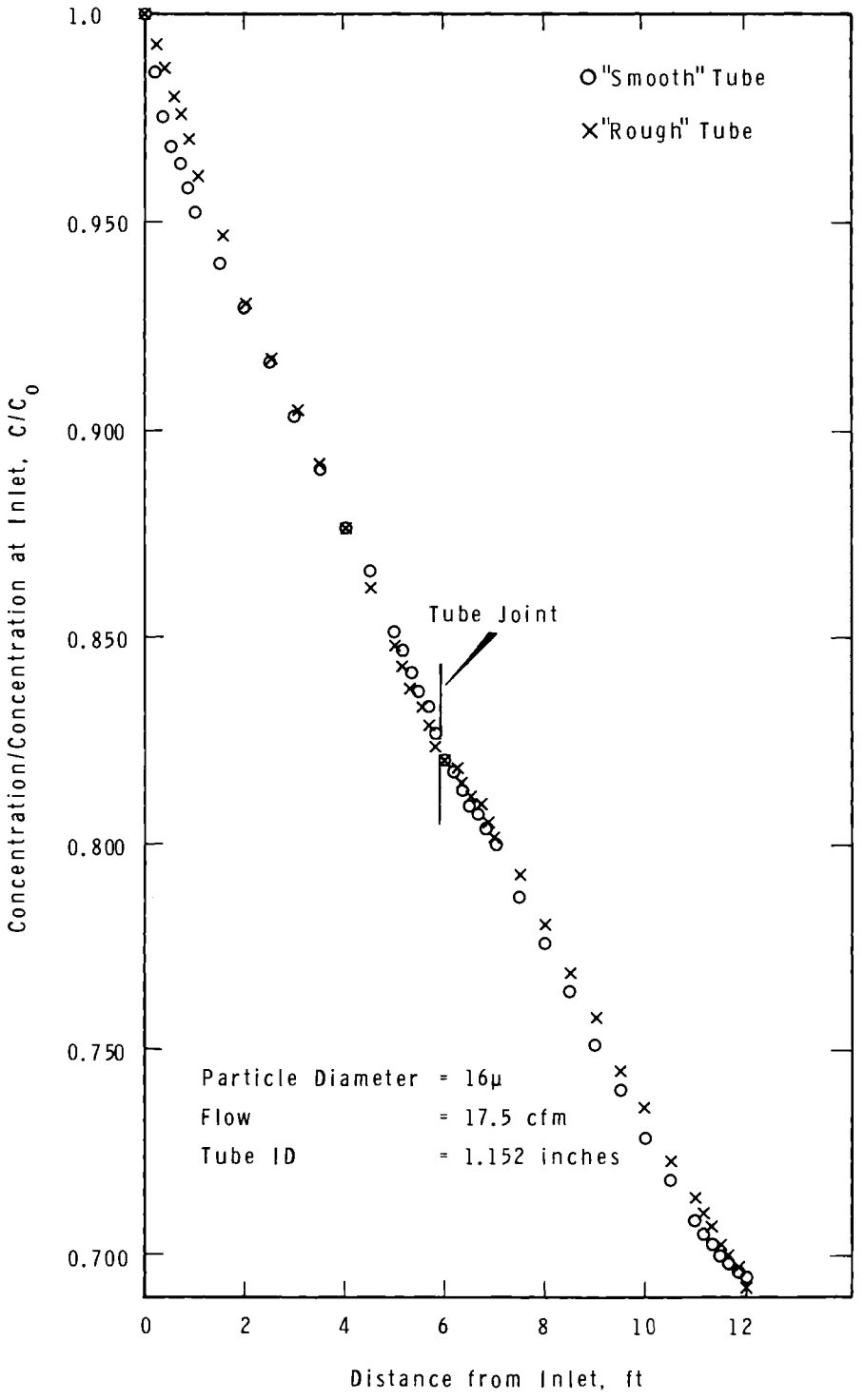

Neg 0672863-5

FIGURE 8. Aerosol Concentration Profiles Showing the Change in Deposition at a Tube Joint

t = time, sec

u = velocity of gas in axial direction at any point, cm/sec

u^+ = u/u_*, dimensionless

u_* = friction velocity, $V\sqrt{f/2}$ = $\sqrt{\tau_o/\rho}$, cm/sec

v = component of $\vec{v}$, cm/sec

$\vec{v}$ = vector velocity of gas at any point, cm/sec

v_o = assumed equal to a root mean square of the radial component of the fluctuating gas velocity, taken as $0.9\ V\sqrt{f/2}$, cm/sec (Ref. 1)

V = average axial velocity in tube, cm/sec, also volume containing continuity system, cm^3

x = rectangular coordinate parallel to solid wall and in the direction of flow, cm

y = distance from tube wall in rectangular coordinate, cm

y^+ = distance from tube wall, $y\,u_*/\nu$, dimensionless

Z = cylindrical coordinates along tube axis, cm

δ_i = unit vector, dimensionless

ΔC = $C_2 - C_1$ in which 1 and 2 refer to two control surfaces, particles/cm^3

ϵ = eddy diffusivity of gas, cm^2/sec

ϵ_p = eddy diffusivity of particles, cm^2/sec

$\varkappa$ = "universal" constant in Equation (20)

θ = angle in cylindrical coordinates

μ = gas viscosity, g/(cm sec)

ν = kinematic viscosity, μ/ρ, cm^2/sec

ρ = gas density, g/cm^3

ρ_p = particle density, g/cm^3

τ = particle relaxation time, $\rho d^2/(18\mu)$, sec

$\underline{\underline{\tau}}(t)$ = shear stress tensor, g force/cm^2

τ_o = shear stress at tube wall interface, g force/cm^2

τ_p = momentum flux at tube wall associated with deposition particles, g force/cm^2

τ_s = shear at gas-solid interface due to momentum flux at tube wall, g force/cm^2

τ_{xy} = shear stress exerted in the x-direction on a fluid surface of constant y by the fluid in the region of lesser y, g force/cm^2

∇ = the vector-operator "del" defined in Equation (5)

Overline

$\overline{\qquad\qquad}$ time smoothed

Superscript

' deviation from time smoothed value

Subscript

r = radial direction

x = direction of average flow parallel to solid wall

y = direction perpendicular to the average flow in the x-direction

z = axial direction in cylindrical coordinates

Substantial Time Derivative in Rectangular Coordinates

$$\frac{DC}{Dt} = \frac{\partial C}{\partial t} + v_x \frac{\partial C}{\partial x} + v_y \frac{\partial C}{\partial y} + v_z \frac{\partial C}{\partial z}$$

REFERENCES

1. S. K. Friedlander and H. F. Johnstone. "Deposition of Suspended Particles from Turbulent Gas Streams," Ind. Eng. Chem., vol. 49, pp. 1151-1156. 1957.

2. P. R. Owen. "Dust Deposition from a Turbulent Airstream," Int. J. Air-Water Pollution, vol. 3, pp. 8-25, 50-53. 1960. Also in Aerodynamic Capture of Particles, edited by E. G. Richardson, Pergamon Press, New York, 1960, pp. 8-25, 50-53.

3. C. N. Davies. "The Rate of Deposition of Aerosol Particles for Turbulent Flow Through Ducts," Ann. Occup. Hyg., vol. 8, pp. 239-245. 1965.

4. C. N. Davies. "Deposition of Aerosols from Turbulent Flow Through Pipes," Proc. R. Soc. A., vol. 289, pp. 235-246. London, 1966.

5. C. N. Davies. Aerosol Sciences, Academic Press, Inc., New York, New York, 1966, pp. 425-440.

6. M. I. Yudine. "Physical Considerations of Heavy-Particle Diffusion," Advances in Geophysics, vol. 9, pp. 185-191. 1959.

7. N. Fuchs. The Mechanics of Aerosols, The MacMillan Company, New York, New York, 1964. pp. 70 and 264.

8. E. G. Pereles. The Theory of Dust Deposition from a Turbulent Airstream by Several Mechanisms, Safety in Mines Research Establishment, Res. Report No. 144. Great Britain, 1958.

9. Perry's Chemical Engineers Handbook, McGraw Hill Cook Co., Inc., New York, 1950, 3rd ed., p. 382.

10. T. S. Kress and F. H. Neill. A Model for Fission Product Transport and Deposition under Isothermal Conditions, ORNL-TM-1274. Oak Ridge National Laboratory, Oak Ridge, Tennessee, October 1965.

11. T. S. Kress. Parameters of Isothermal Fission Product Deposition, ORNL-TM-1330. Oak Ridge National Laboratory, Oak Ridge, Tennessee, December 1965.

12. M. N. Ozisik. "A Heat-Mass Analogy for Fission-Product Deposition from Gas Streams," Trans. ANS, vol. 6, pp. 265-267. 1963.

13. M. N. Ozisik. An Analytical Model for Fission Product Transport and Deposition from Gas Streams, ORNL-3379. Oak Ridge National Laboratory, Oak Ridge, Tennessee, August 1963.

14. M. N. Ozisik. Temperature Effects on Fission-Product Deposition, ORNL-3542. Oak Ridge National Laboratory, Oak Ridge, Tennessee, 1964.

15. G. E. Raines. Mathematical Models of Fission-Product Deposition and the Correlation of Experimental Data, BMI-X-278. Battelle Memorial Institute, Columbus, Ohio, March 1964.

16. R. B. Bird, W. S. Stewart and E. N. Lightfoot. Transport Phenomena, John Wiley & Sons, Inc., New York, New York, 1962. 2nd ed., [16a] p. 5, [16b] p. 159, [16c] p. 161, [16d] p. 723, [16e] p. 726.

17. V. F. Fitz Patrick, S. M. Nielson, and L. C. Schwendiman. Particle Deposition in a One-Half Inch Conduit, HW-73404. Hanford Laboratories, Richland, Washington, June 1962.

18. S. K. Friedlander. "Principles of Gas-Solids Separation in Dry Streams," Chem. Eng. Progress Symposium Series, no. 25, vol. 55, pp. 146-147. 1959.

19. L. C. Schwendiman, G. A. Sehmel, and A. K. Postma. Radioactive Particle Retention In Aerosol Transport Systems. (Published in the Proceedings of the International Conference on the Radioactive Pollution of Gaseous Media at Saclay, France, November 12-16, 1963. Sponsored by the French Section of the Health Physics Society, Presses Universitaires de France, Parish, pp. 373-385.) HW-SA-3210, Hanford Laboratories, General Electric Company, Richland, Washington, October 1963.

20. L. C. Schwendiman and A. K. Postma. "Turbulent Deposition in Sampling Lines," HW-SA-2286 and TID-7627, pp. 127-136. Hanford Laboratories, Richland, Washington, September 1961.

21. G. A. Sehmel and L. C. Schwendiman. "The Turbulent Transport and Deposition of Particles Within Vertical Conduits," Proceedings of the Eighth AEC Air Conference, Oak Ridge, Tennessee, October 22-25, 1963, USAEC Report TID-7677, pp. 653-663. 1963. HW-SA-3183, Hanford Laboratories, Richland, Washington, October 1963.

22. N. Stavropolous. Deposition of Particles from Turbulent Gas Streams, Columbia University, 1957. (M. S. thesis in Chem. Eng.)

23. A. C. Wells. "Transport of Micron-sized Droplets to Vertical Surfaces," Health Physics and Medical Division Research Progress Report for January-December, 1966, AERE-PR-HPM-9, p. 1. Atomic Energy Research Establishment, Harwell, Great Britain, 1966.

24. M. Poreh. Diffusion from a Line Source in a Turbulent Boundary Layer, Colorado State University, 1962. (Ph. D. thesis in Engineering Mechanics)

25. C. M. Tchen. "Diffusion of Particles in Turbulent Flow," Advances in Geophysics, vol. 9, pp. 165-174. 1959.

26. P. G. Saffman. "Flow of a Dusty Gas Between Rotating Cylinders," Nature, vol. 193, pp. 463-464. 1962.

27. P. G. Saffman. "The Life on a Small Sphere in a Slow Shear Flow," J. Fluid Mech., vol. 22, pp. 385-400. 1965.

28. H. H. Chiu. Boundary Layer Flow with Suspended Particles, Report PB 163717. Princeton University, Clearinghouse for Federal Scientific & Technical Information, 1962.

29. V. Goldschmidt and S. Eskinazi. "Two-Phase Turbulent Flow in a Plane Jet," J. of Applied Mechanics, vol. 33, pp. 735-747. 1966.

30. S. C. Wakstein. The Motion of Small Particles Suspended in Turbulent Air Flow in a Vertical Pipe, Queen Mary College, University of London, 1966. (Ph. D. thesis)

31. A. K. Postma and L. C. Schwendiman. Studies in Micromeritics -- Particle Deposition in Conduits as a Source of Error in Aerosol Sampling, HW-65308. Hanford Laboratories, Richland, Washington, May 1960.

32. C. S. Lin and R. W. Moulton. "Mass Transfer Between Solid Walls and Fluid Streams," Ind. Eng. Chem., vol. 45, pp. 636-640. 1953.

33. J. Laufer. "The Structure of Turbulence in Fully Developed Pipe Flow," National Advisory Committee for Aeronautics Research Report 1174, National Bureau of Standards, 1954.

34. W. G. Schlinger and B. H. Sage. "Material Transfer in Turbulent Gas Streams," Ind. Eng. Chem., vol. 45, pp. 657-661. 1953.

35. G. A. Sehmel. "The Density of Uranine Particles Produced by a Spinning Disc Aerosol Generator," Amer. Ind. Hyg. Assoc. J., Sept.-Oct., 1967. pp. 491-492.

36. H. L. Greene and W. R. Lane. Particulate Clouds, Dusts, Smokes, and Mists, D. Van Nostrand Co., Inc., Princeton, New Jersey, 1964. 2nd ed., fig. 2.13, plate 2.

37. P. R. Owen. "Saltation of Uniform Grains in Air," J. Fluid Mech., vol. 20, pp. 225-242, 1964.

38. R. L. Walker and B. R. Fish. Adhesion of Particles to Surfaces in Liquid and Gaseous Environments, ORNL-TM-1228. Oak Ridge National Laboratory, Oak Ridge, Tennessee, August 1965.

39. G. A. Sehmel. "Particle Deposition and Re-entrainment in Long Vertical Conduits," Pacific Northwest Laboratory Annual Report for 1965, in the Physical Sciences, BNWL-235-3, pp. 61-64. Pacific Northwest Laboratory, Richland, Washington, May 1966.

40. L. F. Epstein and T. F. Evans. Deposition of Matter from a Flowing System, GEAP-4140. General Electric Company, San Jose, California, December 1962.

41. M. Corn and F. Stein. "Re-Entrainment of Particles from a Plane Surface," Amer. Ind. Hyg. Assoc. J., vol. 26, pp. 325-336. 1965.

42. A. Pfeiffer. "Rebound of Liquid Drops from a Solid Surface," Amer. Ind. Hyg. Assoc., J., vol. 26, pp. 579-584. 1965.

43. P. Bock. "Some Physical Aspects of Flow Near Surfaces," Trans. N. Y. Acad. Sc., vol. 25, pp. 902-918. 1963.

44. P. Bradshaw. "Irrational Fluctuations Near a Turbulent Boundary Layer," J. Fluid Mech., vol. 27, pp. 209-230. 1967.

45. M. E. O'Neil and K. Stewartson. "On the Slow Motion of a Sphere Parallel to a Nearby Plane Wall," J. Fluid Mech., vol. 27, pp. 705-724. 1967.

46. P. W. Runstadler, S. J. Kline and W. C. Reynolds. An Experimental Investigation of the Flow Structure of the Turbulent Boundary Layer, AFOS-R-5241, Standard University, California, June 1963.

47. G. Segre and A. Silberberg. "Behavior of Macroscopic Rigid Spheres in Poiseuille Flow," J. of Fluid Mech., vol. 14, pp. 136-157. 1962.

48. G. A. Sehmel. "Particle Flux Profiles in Turbulent Flow," "Particle Deposition within a Curved Sampling Probe," "Errors Arising from Anisokinetic Sampling of Particles Flowing in a Conduit," "Particle Deposition and Re-entrainment in Vertical Conduits," Pacific Northwest Laboratory Annual Report for 1966 in the Physical Sciences, BNWL-481-3. Pacific Northwest Laboratory, Richland, Washington, 1967.

49. G. A. Sehmel. Validity of Air Samples as Affected by Anisokinetic Sampling and Deposition Within the Sampling Line, BNWL-SA-1045. Pacific Northwest Laboratory, Richland, Washington, April 1967.

50. F. Kreith and O. K. Sonju. "The Decay of a Turbulent Swirl in a Pipe," J. Fluid Mech., vol. 22, pp. 257-271. 1965.

51. W. T. Sproull. "Viscosity of Dusty Gases," Nature, vol. 190, pp. 976-978. 1961.

52. J. W. Thomas. "Gravity Settling of Particles in a Horizontal Tube," J. APCA, vol. 8, pp. 32-34. 1958.

53. G. A. Sehmel. Subisokinetic Sampling of Particles in an Air Stream, BNWL-217. Pacific Northwest Laboratory, Richland, Washington, March 1966.

54. V. M. Berezhnoi and V. V. Kirichenko. "Theory of Diffusive Deposition of Decay Products of Inert Gases in Circular and Flat Conduits," Soviet Atomic Energy, vol. 17, no. 4, pp. 1031-1034. 1964.

55. L. P. Davis. Deposition of Submicron Size Particles in Ventilation Ducts, ORNL-TM-873. Oak Ridge National Laboratory, Oak Ridge, Tennessee, May 1964.

56. J. D. Dawes and A. Slack. "Deposition of Airborne Dust in a Wind Tunnel," Safety In Mines Research Establishment, Res. Report No. 105. Great Britain, 1954.

57. T. F. Evans. Deposition of Matter from a Flowing Stream, GEAP-4141. General Electric Company, San Jose, California, December 1962.

58. R. I. Mitchell, R. E. Thomas, and J. M. Pilcher. "Transport of Aerosols Through Ducts," Ind. Eng. Chem., vol. 3, pp. 339-345. 1964.

59. A. C. Chamberlain. Transport of Particles Across Boundary Layers, AERE-M-1122. Atomic Energy Research Establishment, Harwell, Great Britain, November 1962.

60. A. C. Chamberlain. "Transport of Gases to and from Grass and Grass-Like Surfaces," Proc. R. Soc., A., vol. 290, pp. 236-265. London, 1966.

61. A. C. Chamberlain. "Transport of Lycopodium Spores and Other Small Particles to Rough Surfaces," Proc. R. Soc., vol. 296, pp. 45-70. London, 1967.

62. H. L. Fisher, Deposition Velocities of Aerosols and Vapors on Pasture Grass, UCRL-14702. Lawrence Radiation Laboratory, Livermore, California, March 1966.

63. G. A. Sehmel. Estimation of Air Stream Concentration of Particulates from Subisokinetically Obtained Filter Samples, BNWL-SA-303. Pacific Northwest Laboratory, Richland, Washington, April 1966.

64. G. A. Sehmel. "Errors in the Subisokinetic Sampling of an Air Stream" Ann. Occup. Hyg., vol. 10, pp. 73-78. 1967.

65. R. E. Davis. "The Visual Examination of Gas Flow Round Pipe Bends Using a New Aerosol Technique," Int. J. Air-Water Pollution, vol. 8, pp. 177-184. 1964.

66. J. H. Horlock. "Some Experiments on the Secondary Flow in Pipe Bends," Proc. R. Soc. A., vol. 234, pp. 335-346. London, 1956.

67. C. N. Davies. "Brownian Deposition of Aerosol Particles from Turbulent Flow Through Pipes," Proc. R. Soc. A., vol. 290, pp. 557-562. London, 1966.

68. I. B. Wilson. "The Deposition of Charged Particles in Tubes, with References to the Retention of Therapeutic Aerosols in the Human Lung," J. of Colloid Science, vol. 2, pp. 271-276. 1947.

69. J. D. Yoder and L. Silverman. "Influence of Turbulence on Aerosol Agglomeration and Deposition in a Pipe," paper no. 67-33, 60th Annual APCA meeting, Cleveland, Ohio, June 13, 1967.

DISTRIBUTION

No. of Copies	
1	AEC Chicago Patent Group G. H. Lee R. K. Sharp
5	AEC Division of Biology and Medicine Germantown, Washington, D. C. R. Beadle
339	AEC Division of Technical Information Extension
1	AEC Idaho Falls Operations Office Idaho Falls, Idaho 83401 H. J. Paas, Jr.
3	AEC Richland Operations Office Technical Information Library (2) C. L. Robinson
1	Air Pollution Technical Information Center National Center for Air Pollution Control Public Health Service, DHEW Washington, D. C. 20201 Mrs. Mary C. Holland
2	Atlantic Richfield Hanford Company D. J. Brown W. P. McCue
4	Battelle Memorial Institute R. I. Mitchell Extra (3)
1	Department of Army Bldg. 3330, Edgewood Arsenal Edgewood Arsenal, Maryland 21010 G. Asset
2	Department of Health, Education & Welfare National Center for Air Pollution Control 4676 Columbia Parkway Cincinnati, Ohio 45226 W. A. Cote J. S. Nader
1	Donald W. Douglas Laboratory M. L. Smith

2 Hanford Environmental Health Operation

F. E. Adley
R. J. Uhle

1 Harvard School of Public Health
665 Huntington Avenue
Boston, Massachusetts 02115

P. C. Reist

1 Lawrence Radiation Laboratory
Livermore, BML (AEC)

R. Yoder

1 Los Alamos Scientific Laboratory

H. F. Schulte

1 Oak Ridge National Laboratory
Oak Ridge, Tennessee 37830

L. F. Parsly

1 University of Rochester (Simon)

T. T. Mercer

1 U. S. Department of Argiculture, Agriculture Research Service
National Animal Disease Laboratory
P. O. Box 70
Ames, Iowa 50011

J. R. Sanger

75 Battelle-Northwest

W. J. Bair
J. R. Bovingdon
J. P. Corley
G. M. Dalen
W. E. Davies
W. L. Dotson
C. E. Elderkin
J. J. Fuquay
D. I. Hagen
W. T. Hines
R. L. Junkins
K. H. Larson
P. W. Nikola
R. S. Paul
A. K. Postma
R. W. Perkins
E. H. Phinney
L. C. Schwendiman
G. A. Sehmel (50)
C. L. Simpson
B. D. Stuart
Technical Information Files (4)
Technical Publications